CHALMERS
UNIVERSITY OF TECHNOLOGY

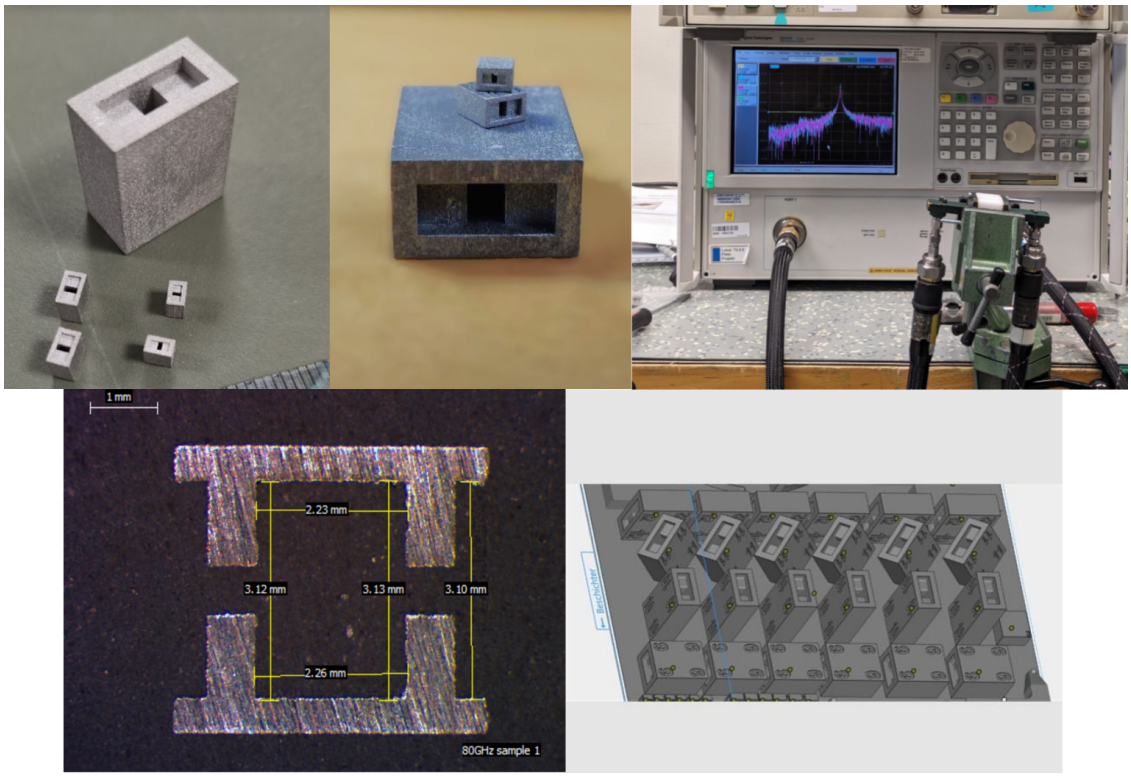

PRECISION MANUFACTURING USING ADDITIVE MANUFACTURING

A Study Exploring the Possibility of Additive Manufacturing of Metallic Structures in Microwave Radio Links and 5G Base Stations using Binder-Jetting and Material-Jetting.

ABHINAV SATHI PRAVEEN

SOHAM BHATTACHARYYA

DEPARTMENT OF INDUSTRIAL AND MATERIAL SCIENCE

CHALMERS UNIVERSITY OF TECHNOLOGY
Gothenburg, Sweden 2024
www.chalmers.se

Master's thesis 2024

Precision Manufacturing Using Additive Manufacturing

A Study Exploring the Possibility of Additive Manufacturing of Metallic Structures in Microwave Radio Links and 5G Base Stations using Binder-Jetting and Material-Jetting.

ABHINAV SATHI PRAVEEN
SOHAM BHATTACHRYYA

CHALMERS
UNIVERSITY OF TECHNOLOGY

Department of Industrial and Material Science
Division of Materials and Manufacturing
Chalmers University of Technology
Gothenburg, Sweden 2024

Precision Manufacturing Using Additive Manufacturing.
A Study Exploring the Possibility of Additive Manufacturing of Metallic Structures in Microwave Radio Links and 5G Base Stations using Binder-Jetting and Material-Jetting.
Abhinav Sathi Praveen
Soham Bhattacharyya

Supervisor: Torbjörn Westin, Ericsson
Examiner: Lars Nyborg, Department of Industrial and Material Science

Master's Thesis 2024
Department of Industrial and Material Science
Division of Materials and Manufacturing
Chalmers University of Technology
SE-412 96 Gothenburg
Telephone +46 31 772 1000

Cover: (Top row from left to right): Binder Jet (Left) and Material Jet(right) showcasing variation in size of different frequencies; Vector Network Analyser(VNS) test setup for 23GHz; (bottom row from left to right): Cross-sectional view of the 80GHz sample; Binder jetting bed layout for different orientations.

Typeset in LaTeX
Gothenburg, Sweden 2024

Precision Manufacturing Using Additive Manufacturing
A Study Exploring the Possibility of Adittive Manufacturing of Metallic Structures in Microwave Radio Links and 5G Base Stations using Binder-Jetting and Material-Jetting.
Abhinav Sathi Praveen
Soham Bhattacharyya
Department of Industrial and Material Science
Chalmers University of Technology

Abstract

With the increase of global data traffic every year, the demand for high-speed connectivity is getting stronger day by day. Microwave technology for wireless communication is a strong contender for high-speed, low-latency communication. These high frequency transmission links have tiny cavity filters with complex geometry, which is arduous to manufacture with the conventional methods. This calls for novel alternative manufacturing technologies to produce these filters without compromising the performance. The thesis explores the feasibility of employing additive manufacturing techniques called binder jetting (BJT) and Material Jetting (MJT) for the manufacturing of the tiny intricate cavity resonators for 23GHz, 80GHz, and 110GHz respectively. The resonators were manufactured by Bosch using Markforged PX100™ BJT printer and XJET Caramel 1400M MJT printer with different orientations to study electrical performance and how dimensional accuracy and surface roughness affect the performance of the printed parts. The print job for the BJT was carried out in two batches, second print was carried out after making the design changes from the feedback of the first print. The first design presents itself with sharp edges and corners while the second one incorporates fillets. The design change has brought difference in the results as well, the first print showed a close resonant frequency with less output signal while the second print with fillets shows a shift in anticipated frequency but with improved output signal. MJT parts reproduced the designed resonant frequency with superior surface finish and dimensional accuracy. It is unclear that the different orientations have effect on the performance of the resonator.

Keywords: Additive Manufacturing, cavity resonators, Binder jetting, Material jetting, q factor, surface roughness, dimensional accuracy.

Acknowledgements

This master thesis project was carried out at the mechanical and thermal division under the hardware department at Ericsson Gothenburg, as part of our master studies in Materials Engineering at Chalmers University of Technology. First, we would like to thank both parties for facilitating us with the opportunity to be part of this study.

We express our sincere gratitude to our supervisor Torbjörn Westin for his constant encouragement, positivity, informative advice and feedback throughout our journey. We would like to acknowledge the efforts put by Thanh Do A and Thomas Emanuelsson for helping us with the understanding, measurements and characterization of the electrical performance of the resonators. Also, we thank Bosch, X-JET, Amexci, and other stakeholders who helped us in printing the parts. Special thanks to our examiner Lars Nyborg for providing us constant support throughout the project.

Finally, we would like to acknowledge our family, friends, and other well wishers for their constant support for the whole duration of our course.

Abhinav Sathi Praveen, Gothenburg, June 2024
Soham Bhattacharyya, Gothenburg, June 2024

List of Acronyms

Below is the list of acronyms that have been used throughout this thesis listed in alphabetical order:

ABS	Acrylonitrile Butadiene Styrene
AlSi	Aluminum Silicon
AM	Additive Manufacturing
BJT	Binder Jet
CAD	Computer Aided Design
DOD	Drop on Demand
DRIE	Deep reactive Ion Etching
HIP	Hot Isotactic Pressing
LBM	Laser Beam Machining
LMM	Lithography-based Metal Manufacturing
LOM	Light optical microscopy
LPS	Liquid phase sintering
MEMS	Micro-Electro-Mechanical Systems
NPJ	Nanoparticle Jetting
PA	Polyamide
PA-CF	Polyamide with Carbon fiber reinforcement
PBEB	Powder bed fusion Electron Beam
PBFLM	Powder bed fusion Laser Beam Metal
PC	Polycarbonate
PLA	Polylactic Acid
SLPS	Supersolidus liquid phase sintering
SMA	Shape Metal Alloys
SS	Solid state sintering
TPU	Thermoplastic Polyurethane

Contents

List of Figures

List of Tables

1
Introduction

The chapter gives an overview of the project setting from the Ericsson standpoint. In addition, it discusses the aim, limitations & delimitations, and the questions that the thesis will address by the end of the project.

1.1 Background

Ericsson is one of the world's leading networking and telecommunications giant based in Sweden. This master thesis is conducted in the Department of "Mechanical and Thermal Design" under the hardware unit at Ericsson Lindholmen, Göteborg.

With global data traffic increasing every year, the demand for high-speed connectivity increases every second (Ericsson, 2021). Ericsson's vision is to provide limitless connectivity that improves lives, redefines business, and pioneers a sustainable future (Ericsson, ndb). Ericsson's 5G technology efficiently supports this growth and demand for data. Ericsson MINI-LINK 6000 enables hassle-free 5G network transportation, which covers the entire spectrum from 5GHz to 80GHz (Ericsson, nda). The low power, low latency, cost efficient and high-capacity solution is achieved using microwave technology(Ericsson, nda).

This technology can replace the fibers, where laying fibers can be expensive and impractical, without compromising the data transfer rate (Ericsson, 2021). The high frequency transmissions links contain tiny cavity filters having complex geometries, which are getting difficult to manufacture using conventional methods. For future products, Ericsson wants to explore the possibility of employing alternative novel manufacturing techniques to produce these cavity filters.(Zhang and Zirath, 2016)

Ericsson initiated its AM research program to improve its understanding of additive manufacturing, circulate this knowledge, and explore how the technology can be leveraged to benefit the company. Furthermore, Ericsson sees additive manufacturing as a potential contributor to its aim of achieving carbon neutrality by 2030(RISE, 2022).

1.2 Aim

In future, Ericsson wants to use additive manufacturing (AM), wherever possible to produce the parts, as it has high dimensional freedom, less material wastage, and

can be locally produced faster for small volumes thus bringing the production closer to people. The company wants to study possible additive manufacturing (AM) techniques to manufacture parts for network transport links.

Our project aim is to provide a detailed study report on various techniques like binder jetting technique (BJT), and nanojetting to produce cavity resonators of frequency 23GHz, 80GHz, and 110GHz network links. This includes studying and comparing the surface finish, dimensional accuracy, and electrical performance of different additive manufactured components. The successful thesis work could open the possibility of new manufacturing techniques and expand the product portfolio with higher frequency network links.

1.3 Limitations

The Study was supposed to be done with different materials such as aluminum, copper, stainless steel using different printing techniques. However, due to supplier and logistic limitations, the BJT and MJT processes explored could only print stainless steel material. This made the experimental comparison study on materials difficult, allowing to compare stainless steel with respect to all parameters and the rest of the materials with the help of literature. The repeatability of the manufacturing process cannot be verified due to printer availability and time constraints, as multiple printing sessions are not possible.

1.4 Delimitations

The study focuses solely on the printing step and processes. In this study, post-processing methods are not explored. Only BJT and MJT printing processes are being investigated. The printed specimens are only tested for surface roughness, dimensional accuracy, and electrical compatibility test. No test regarding mechanical strength is done on the specimen. For an easier comparison, the process and print parameters like hatch distance, print speed, laser power, etc. are kept constants for all prints on a specific machine.

1.5 United Nations Sustainable Development Goals (SDG)

This study, has a potential to address these 4 of the 17 SDGs listed by UN (United Nations Development Program, 2023).

SDG 4 – Quality Education
The technology has the potential to provide high-speed Internet connectivity in remote areas, facilitating access to online resources, virtual classrooms, and other

interactive learning platforms such as virtual reality.

SDG 09 - Industry, Innovation, and Infrastructure
§ The study will help to foster innovation in the communication industry by exploring additive manufacturing to manufacture high frequency network transport link parts.

SDG 10 – Reduced Inequalities
In countries with tight economic constraints, 2G and 3G networks prevail. There are barriers to the deployment of the 5G network. That includes high infrastructure costs, device affordability, regulatory and adoption requirements. This technology will help to expand the connectivity to remote areas, where the installation of optical fiber cables is expensive and impractical, thus making the Internet accessible to everyone.

SDG 12 - Responsible Consumption and Production
Additive manufacturing process has less material wastage compared to milling and powders can be reused, making production and material consumption more sustainable.

1.6 Research Questions

This thesis will answer the following research questions.

- Which additive manufacturing methods could fulfill the dimensional requirements for high frequency network filter applications?
- How will the surface roughness of the printed part affect the Q-factor of the electrical resonator?
- How will the dimensional accuracy of the printed part affect the achieved frequency vs the simulated frequency?

2

Literature and State-of-The-Art Study

In the following sections, the literature reviewed for this study is described. It includes information about cavity resonators, various additive manufacturing technologies, post-processing technologies available in the industry, alternate manufacturing solutions and various characterisation techniques that could be used.

2.1 Frequency filters and cavity resonators

A cavity filter or a resonator is either a hollow or a dielectric enclosed within a metal structure which act as a band pass filter. The filter design functions by selecting a particular frequency and rejecting others. The cavity has a resonant frequency at which it most efficiently selects a certain frequency signal. This frequency can be tuned by altering the dimension of the cavity(Paschotta, 2007).

A cavity resonator was chosen for the study to better understand the performance and behavior of the filter on a unit level when additive manufactured.

Its characteristics include high selectivity, low loss, and the ability to handle high power. This makes these resonators to be used in filters for a wide variety of applications in microwave and millimeter wave systems, which require high Q or Quality-factor and low insertion loss(RF, 2022).

Quality factor or Q-factor measures how much a resonator is close to an ideal cavity resonator. An ideal resonator will sustain the oscillations for an infinite amount of time. In reality, the resonators sustain the oscillations for a finite amount of time. This is due to radiation losses, dissipation losses in the dielectric medium, or resistive losses from the material of the cavity. The high Q-factor indicates better performance with discrete narrow bandwidth.

Another important parameter in cavity resonator is the insertion loss (IL). It refers to the power loss experienced while the signal passes through the cavity(Zhang and Zirath, 2016). The IL increases with increase in frequency(Gold and Helmreich, 2017).

2.2 Additive Manufacturing Technologies

Classification of AM technologies is often confusing and can be misleading. To address that challenge, this report will stick to the classification mentioned in the ISO standard.

According to ISO / ASTM 52900:2021, Additive Manufacturing is defined as a material addition process where the material is added in a layer by layer fashion to manufacture a three dimensional part in contrast to the traditional substractive way where material is removed from a larger volume of material. The part may or may not require support material depending on the geometry and the type of process. Additive manufacturing processes can be divided into the following categories:

2.2.1 Binder Jetting (BJT)

"*It is described as an additive manufacturing process in which a liquid bonding agent is selectively deposited on a powder bed to hold the powder together.* In this state, the part retains dimension, but lacks strength or integrity. It is called a 'green part'(Gibson et al., 2020). It is followed by removal of unbound powder and a sintering process which could be a single step or multi step process. There is a wide range of materials in metals, polymers, composites, and ceramics that can be utilized using this process. The interesting materials for this thesis work involves metals especially Cu, An infiltration process may be deployed to fill up pores and voids to modify the properties of the base part like the density, high strength and a better control over dimensional accuracy.(Gibson et al., 2021).
An interesting relation is the requirement of high-volume fraction packing which could be attained by adjusting powder morphology or increasing the Powder Size Distribution (PSD) resulting in smaller sized particles effectively filling gaps between the larger one. This is required for better 'green part' handling, but could also favor the requirement of superior surface finish.

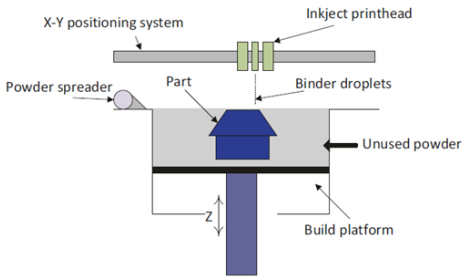

Figure 2.1: Schematics of the BJT process. Taken from (Gibson et al., 2021).

This process enables higher productivity and throughput rates due to the ab-

sence of the requirement of supports and the ability to stack up parts in the entire build volume.

2.2.2 Direct Energy Depostion (DED)

"*Additive manufacturing process in which focused thermal energy is used to fuse materials by melting as they are deposited.*" This technology is preferred predominantly for metal powders. DED differs from Powder Bed Fusion (PBF) due to the absence of a pre-laid powder in a bed. The usual energy sources include Laser or electron beam, friction stirring or an arc. The build up process is synonymous to Material Extrusion (MEX). The machines in the market differ in terms of Laser power, laser spot size, laser type, powder delivery method, feedback control, and type of motion. Some of the manufacturer specific processes go by the names, Laser Engineered Net Shaping (LENS), Direct metal deposition (DMD), Laser-Based material deposition (LBMD), Laser Freeform Fabrication (LFF) etc. The part is fabricated onto a substrate, usually a plate. The fabrication takes place using differential motion between the printing head and the substrate. The actuation is achieved by a 3, 4 or 5 axis system (Gibson et al., 2021).

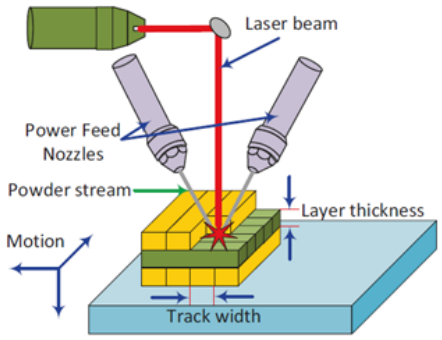

Figure 2.2: Schematics of the DED process. Taken from (Gibson et al., 2021)

A noteworthy observation is the use of high powered energy sources featured to manufacture parts quickly at the cost of geometric precision. Layer thickness range from 0.2 to 4 mm leading to much rough surface compared to PBF (Gibson et al., 2021).

2.2.3 MEX (Material Extrusion)

"*Additive manufacturing process in which material is selectively dispensed through a nozzle or orifice.*" Material Extrusion is one of the most prevalent methods of additive manufacturing and has been extensively researched on. The key methods common to any MEX system would be, loading of material, liquification of the material, pressure application to move this material, plotting of

the heading a predefined path in a controlled manner, bonding of material in a coherent fashion to form a solid structure. Support structures may or may not be required based on geometrical requirements. Supports can also be made in material that can be dissolved chemically, post printing by using a compatible solvent or made with a weaker material that could be snapped off (Gibson et al., 2021).

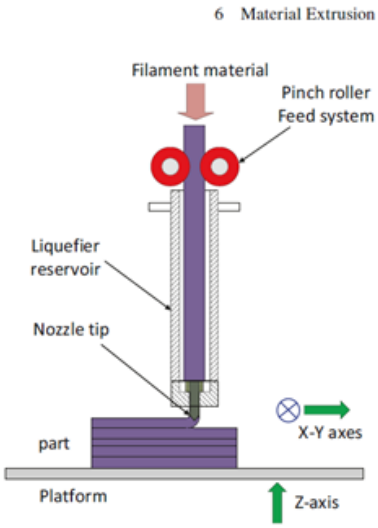

Figure 2.3: Schematics of the MEX process. Taken from (Gibson et al., 2021)

The maximum feature resolution that could be achieved is of order of 0.1mm (Turner and Gold, 2015). For this technology, the dimension accuracy depends on parameters like the accuracy in controlling the material flow rate through the nozzle and thermal mechanisms such as warping and shrinkage. (The most common MEX AM method would be Fuse deposition Modeling (FDM), invented, and developed by Stratasys. MEX technology boasts about low-cost machine components, a library of polymer materials (Thermoplastics and composites). One interesting printer in this category would be Bambu Labs X1 series. It supports materials like PA, PC PA-CF, PLA, TPU and ABS and can print with multiple materials at once and a resolution of 7µm(*https://bambulab.com/en/x1*).

2.2.4 MJT (Material Jetting)

"*Additive manufacturing process in which droplets of feedstock material are selectively deposited.*" This feedstock could be solution or dispersion based. The jetting of material has two modes, i.e. continuous and drop on demand(DOD). Continuous mode ensures high throughput rate. DOD on the other hand, can disperse smaller drop size giving better precision. XJet uses a solution deposition method termed as NanoParticle Jetting™ (NPJ) technology where

fabrication takes place by jetting metallic or ceramic nanoparticles in colloid droplets drizzled using thousands of nozzles. The solvent then evaporates leaving behind the nanoparticles. The technology uses soluble supports which make it quite suitable for the application of Cavity filters. X-Jet claim high dimensional accuracy of 50µm, density greater than 99.5% and a surface roughness of 1.6µm without the requirement of post processing. Current materials include 316L SS and Aluminum Oxide. (*xjet3d.com*)

2.2.5 PBF (Powder Bed Fusion)

"*Additive manufacturing process in which thermal energy selectively fuses regions of a powder bed.*" This additive manufacturing process utilizes thermal energy for selective fusion of designated regions within a powder bed. Following the creation and preheating if necessary of a powder layer, a focused CO_2 laser beam is directed onto the bed. Galvanometers meticulously control the beam's movement, facilitating the thermal fusion of material to establish the desired slice cross-section. Notably, surrounding powder remains unbound, acting as a natural support structure for subsequent layers. This eliminates the requirement for supports, for few characteristic features that other processes need to implement. Upon completion, the fabricated parts are retrieved from the powder bed. Subsequently, any residual, loose powder is removed from the parts. Finally, additional finishing operations may be implemented as deemed necessary (Gibson et al., 2021).

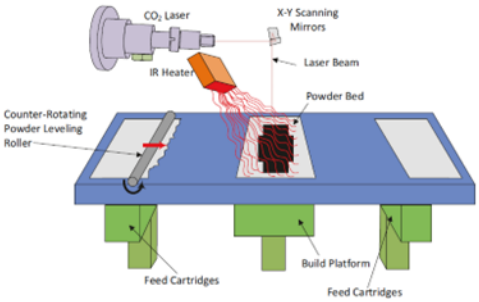

Figure 2.4: Schematics of the PBF process. Taken from (Gibson et al., 2021)

2.2.6 SHL (Sheet Lamination)

"*Additive manufacturing process in which sheets of material are bonded to form a part.*" The sheets can be cut and stacked or the other way around. The varied mechanisms that could be used for the process are thermal bonding, clamping (mechanical interlocking), and ultrasonic bonding (solid state bonding or the blaha effect) (Gibson et al., 2021). The sheet thickness defines the layer thickness in this process and can range from 0.07 to 0.2mm for adhesive bonding. And 100-150µm for ultrasonic bonding. SHL is usually a fast process as the entire layer isn't scanned like other processes rather only the perimeter

is scanned.This allows for the fabrication of large parts. Other advantages of SHL include limited shrinkage and problems due to distortions and residual stresses. As the process works with sheets and not powder, the health and environment hazards are lower (Gibson et al., 2021).

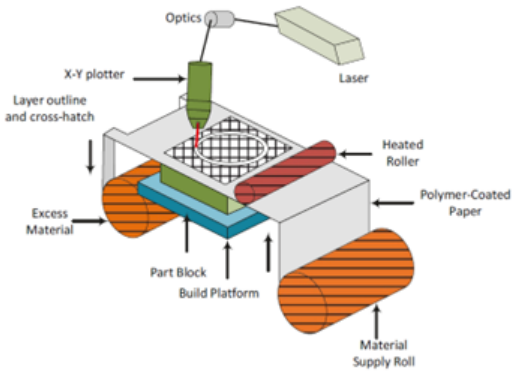

Figure 2.5: Schematics of the SHL process. Taken from (Gibson et al., 2021)

The SHL process has two approaches. 'Bond then form' focuses on bonding a sheet layer first and then cutting out the shape. 'Form then bond' is the right opposite where the layer is first cut out into the required shape and then adhered onto the part. Both processes have their own set of challenges. Hollow parts are hard to form, and the staircase effect often observed in additive manufacturing because of the layer by layer formation of the part is quite prominent, providing an average surface finish.

2.2.7 VPP (Vat Photopolymerization)

"*Process in which liquid photo-polymer in a vat is selectively cured by light-activated polymerization*". The activation of the reaction can be done using direct UV beam exposure, selective UV exposure through a mask or by using LEDs. When it comes to materials, the most commercially available are polymers from the epoxide and acrylate family. The materials available in today's market are usually a hybrid of epoxies and acrylates, where the acrylate contributes to the curing speed and epoxy ensures dimensional accuracy (Gibson et al., 2021).The polymerization initiator could be an UV or an X-ray source. A process named Lithography based Metal Manufacturing (LMM) presents materials consisting of metal powder dispersed in an organic binder. The metal powder could be 316L and 17-4 PH stainless steel, Ti64, Copper or a custom material which could include tungsten, brass, precious metals or a combination of materials. The binder system could be a general purpose binder, or special binder that could be beneficial for dimensional accuracy. Custom binders could also be made based on the requirements. The layer thickness could vary in the range of 10 to 100 µm with a lateral resolution of 40µm. The parts require a sintering process to remove the binder and coa-

lesce the powder and possess a surface roughness of 2µm (Ra) post sintering *incus3d.com*.

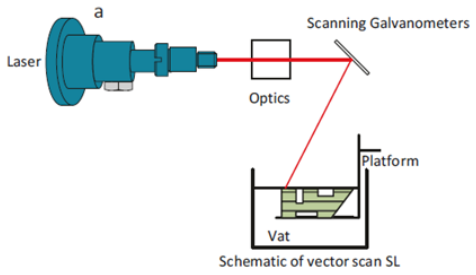

Figure 2.6: Schematics of the VPP process. Taken from (Gibson et al., 2021)

VPP boasts of superior surface finish and dimensional accuracy. A sub process named 'micro vat photopolymerization has been developed for complex shaped parts with size in the range of 1 mm (Gibson et al., 2021).

2.3 AM Process Selection

There are no concrete dimensional requirements or surface roughness for this project. However, there is a need to manufacture parts in metal and check for electrical results without opting for post processing. Processes that go for a finer powder and possess min layer thickness with high resolution of printed layer are preferable. In addition, the use of metals as the material and the presence of soluble or support free printing are a requirement.

Among the 7 broad AM processes, BJT, MJT, PBF-L/M and LMM were short listed. SHL is eliminated because of its inability to form hollow parts(Gibson et al., 2021). The DED energy source is high for micro parts and would therefore not lead to dimensionally accurate parts. In addition, the thickness of the layer is quite prominent to have a good surface finish. Metal-based MEX has been done using a 0.5mm nozzle which provides a thick staircase effect (Lieberwirth et al., 2017). This would be detrimental to surface roughness eliminating MEX.

For MJT, an interesting process named "NanoJet" printing was investigated. The process was chosen due to it's ability to print in metal i.e. 316L SS. The ink used in it possess nanoparticles of the metal which is claimed to provide excellent surface properties and accuracy. Soluble supports are used, which would be beneficial for printing cavities.
PBF-L/M was investigated if the parts could be printed at Chalmers. It was confirmed that the geometry presented could not be printed without supports in the EOS M100 or M290.

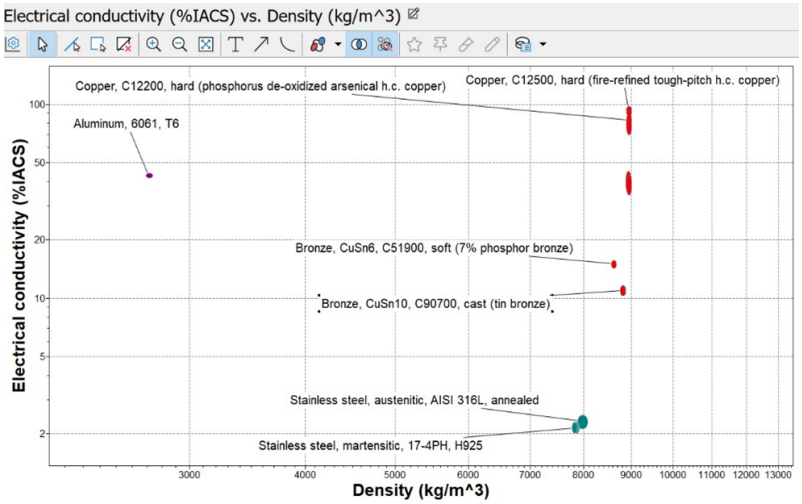

Figure 2.7: plot comparing IACS versus density of the materials in Ansys Granta edupack 2023 R1 .

When it comes to BJT, there were multiple materials that could have been investigated. Ideally, materials with high electrical conductivity is preferred therefore printing in copper was of interest followed by Aluminum, 316L SS and 17-4PH SS as shown in the figure 2.7. The electrical conductivity is measured in IACS% (International Annealed Copper Standard), where the conductivity of annealed copper is considered as 100% IACS at 20°C (established by International Electrotechnical Commission). AMNOVIS and RISE were identified for copper printing. Ricoh could support with Aluminum BJT.

Due to the project circumstances, Bosch's BJT experience was opted and the materials chosen were 316L and 17-4PH. 316L has slightly better electrical properties, on the other hand 17-4PH was easier to control for dimensional accuracy as mentioned by the Bosch team (Bosch, Personal Communication).

2.4 Surface Post Treatment

The primary challenge, additive manufacturing faces when it comes to precision manufacturing is surface morphology. It often lacks the surface quality the conventional manufacturing provides. Surface quality is critical for the performance of the resonator. As the irregularities on the surface can cause conductor loss by disrupting the flow of electric current in the cavity resonators, thus increasing the resistance (Khan and Kuylenstierna, 2024).

Various surface post-treatments are done to improve the surface quality of the AM parts. Surface post treatments can be classified majorly into three groups; they are surface treatments based on material removal, no material removal, coatings, and combination of different treatments (Maleki et al., 2021). Given the focus of this study on AM technologies, the following sections will

exclusively discuss post-treatment methods suitable for resonator components.

2.4.1 Surface post-treatment based on Material Removal

Surface post-treatment based on Material Removal are of two types, they are Machining and chemical treatments.

Machining treatment is done by removing material from the surface to obtain a smooth surface. This is done by chipping out bits of materials from the surface by either machining or by using lasers. Machining or micro-machining, milling and grinding utilizes a cutting tool and a powered machine to remove the materials in a controlled fashion. This process can lower the surface roughness value Ra below 1 μm (Maleki et al., 2021). The major challenge is accessibility of the surface if the part has a complex geometry, especially cavity resonators have structures inside the part which are impossible to reach without slicing the part.

Laser micromachining employs a technique called laser ablation to remove materials from the surface. Unlike conventional machining, no physical contact is happening during the process. This eliminates any mechanically induced material damage or tool damage. By adjusting the pulse duration, one can control the surface finish of the part. The femtosecond pulsed laser can produce surfaces with surface roughness Ra below 1 μm (Maleki et al., 2021).

Another material removal surface treatments are the chemical treatments. Those include chemical etching, chemical polishing, chemical brightening, and electrochemical polishing. The major advantage of the chemical treatments is its ability to treat all the surfaces uniformly. The drawbacks of mechanical machining and laser machining was its inability to access internal surfaces of the cavity. Since chemicals can easily pass through small channels, it is the most sought-after surface treatment technique for parts having complex internal structures.(Maleki et al., 2021)

Most of the chemical treatments are similar in nature. The AM specimen will be kept in a chemical solution at a specific temperature and time duration. The temperature and the duration controls the depth of the material removal (Beevers et al., 2024).

Hirtisation® is a process developed by Hirtenberger Engineered Surfaces (currently RENA Technologies), which is a combination of chemical and electrochemical polishing for additive manufacturing components(Beevers et al., 2024). It is a three-step process consisting of support removal, improving surface roughness, and surface polishing. The specimen is immersed in an electrolyte solution, which participates in the electrochemical reaction for the material removal. The process can target rough areas and sharp edges to pro-

duce a smooth finish effectively. Material removal can be precisely controlled by altering the duration and electrical parameters (Beevers et al., 2024). Being a non-contact process, no mechanical damages are induced during the process, ensuring an excellent repeatability quality finish.

2.4.2 Surface post-treatment based on No Material Removal

This category surface treatments improves the surface quality by inducing plastic deformation on the surface without removing any material. These deformations are induced by mechanical loading, impact loading, or using thermal/kinetic energy. This can affect either the surface or the bulk of the material depending on the process (Maleki et al., 2021). This can again be classified as mechanical and laser-based treatments. Mechanical treatments include rolling, which is the process of deforming the top layer by loading a roller of different shapes and geometries against the specimen (Maleki et al., 2021). Sand blasting is the process of spraying abrasive materials such as sand or beads against the surface under very high pressure(Maleki et al., 2021). Other mechanical treatments include shot peening, cavitation peening, and hot isostatic pressing (HIP); they also improve the hardness of the surface and the fatigue life of the sample along with roughness(Maleki et al., 2021).

2.4.3 Surface post-treatment based on Coatings

Surface coating treatments are used to reduce the roughness or to introduce/enhance certain properties of the part to make it suitable for the use case. The most common coating method used is the electroplating technique. This method involves a reduction reaction where the coating metal ion (anode) in a solution are reduced onto the substrates (cathode) surface using electric current(Simonovic et al., 2022). The material used in electroplating can also introduce new properties like improved mechanical and electrical properties. Silver electroplating can improve the surface conductivity and reduce the insertion loss. Copper plating will also produce good results for the resonator.

The important criteria to do the electroplating is the substrate has to be conductive. To coat non-conductive materials like polymers a chemical method called electroless plating is used. Copper and nickel can be electroless plated to the polymer surface making it conductive to do the electroplating (Eßbach et al., 2021). Electroless plating is an expensive process compared to electroplating. The main challenge of the electroplating is the anode should be able to go through the internal cavities to plate the inside of the cavity(Shukla et al., 2014).

2.5 Alternate Manufacturing Methods

2.5.1 Machining and Laser Micro machining

Unlike conventional machining processes, laser micro machining employs a laser beam to remove extremely small amounts of material, thereby producing minute features. This process relies on a technique known as laser ablation, which involves removing material from the surface of an object through thermal or photochemical erosion(Faisal et al., 2018). As there is no physical interaction between a cutting tool and the material, the process eliminates mechanically induced material damage, tool wear, and tool damage.

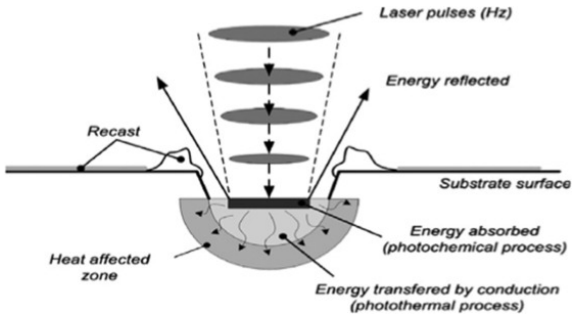

Figure 2.8: Mechanism of the laser pulse and material interaction. [Reproduced by permission of the publisher].

For microfabrication with low tolerance, the laser operates in pulsed mode. This pulsing technique helps minimize thermal damage by reducing the heat-affected zone. Femtosecond pulses are utilized for the manufacturing of resonators, wave guides, and splitters. Additionally, this technology finds applications in the production of micro-electromechanical systems (MEMS), precision cutting, and micro drilling(Sahu et al., 2022).

Laser micromachining can fabricate components with dimensions ranging from 1μm to 1 mm, using materials such as steel, ceramics, and special alloys like shape memory alloys (SMAs). However, challenges include burr and spatter formation, thermal stress, cracking, and surface roughness, which are influenced by the duration of the laser pulse(Maleki et al., 2021).

2.5.2 Deep Reactive Ion Etching

Deep Reactive Ion Etching (DRIE) is a dry etching process that utilizes plasma to generate ions and radicals within a gas mixture, which then bombard the surface to physically remove materials. This technique enables the creation of precise, deep, and narrow structures(Laermer et al., 2020). DRIE primarily comprises two phases: the etching phase and the passivation phase. Initially,

the system surface is etched using a gaseous exchange; the choice of etchant depends on the volatility of the products formed. Gases such as C_4F_8 and CHF_3 form fluoropolymer films on the etched substrate, passivating the side walls and protecting them from further etching(Laermer et al., 2020). This results in an anisotropic process capable of achieving high aspect ratios.

$$\text{Solid} + \text{GaseousEtchant} \longrightarrow \text{VolatileProducts}$$

There are two main DRIE processes. They are the Bosch process and the cryogenic process. The bosch process is a cycling etching method with alternating etching and passivisation. The cryogenic method etches the specimen at very low temperatures around 173K. The cryo temperature will suppress the chemical reaction and etching thus having more controlled etching with smooth surfaces(Laermer et al., 2020). DRIE is particularly effective for etching silicon wafers and other semiconductors. In addition, metals such as aluminum, chromium, and aluminum-copper alloys with less than 4% copper can be etched using chloride gases as etchants. DRIE can achieve aspect ratios of 20:1, where the depth is 20 times the width at the micron level(Laermer et al., 2020).

This technology is essential for the fabrication of MEMS devices, semiconductor components, and waveguides for terahertz applications. For the manufacturing of the waveguides, the DRIE is followed by metal plating. This gives good electrical characteristics, but not very good thermal performance(Malekabadi and Paoloni, 2016). As a clean room technology, DRIE is a complex process and is not compatible with all materials.

2.5.3 LIGA based thick resist electroplating

LIGA is the German acronym for Lithographie (Lithography), Galvanoformung (Electroplating) and Abformung (Molding). It is a process used to fabricate tiny high-aspect ratio structures with precise tolerances. As indicated by its name, LIGA encompasses three stages.(Malekabadi and Paoloni, 2016)

The initial step involves X-ray or UV lithography, in which a thick, light-sensitive photoresist is applied to a substrate. The patterns are then created by exposing the coated substrate to light through a mask. Following lithography, the developed mold undergoes electroplating with a metal, resulting in a structure that replicates the mold's pattern. Subsequently, the remaining photoresist is removed, leaving the metal structures, which can then be used to produce fine structures from metals or polymers through various molding techniques such as injection molding and hot embossing.

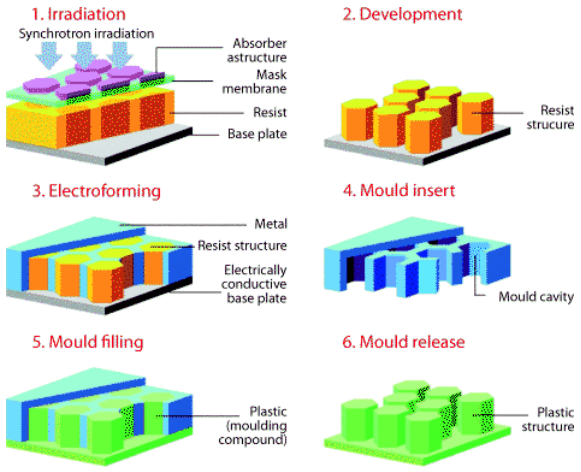

Figure 2.9: Schematics of the LIGA process steps(Cui, 2008) [Reproduced with permission of the publisher].

This process is applicable to the electroplating of metals such as copper, nickel, silver, gold, nickel alloys, copper alloys etc. The SU-8 is a negative photoresist known for its excellent resolution and consistency, and it is frequently used for the fabrication of sub-terahertz (100-1000GHz) waveguides and filters; it also provides a finer surface finish, which is important to obtain good Q-factors.(Malekabadi and Paoloni, 2016)

2.6 Dimensional Accuracy and Surface Texture

Dimensional accuracy and Surface texture of final parts are an important defining characteristic in judging the stability and quality of the process. Dimensional accuracy is defined as the fidelity of the dimensions of a produced part with the ideal required geometry for example the CAD drawing of the part(Leach and Carmignato, 2020).
Some key features in dimensional accuracy include(Elder and Elder, 2022),

1. Flatness: It is defined by how flat a surface is without a reference to any other feature or datum.
2. Surface Perpendicularity: It checks if two surface are at 90° to each other.
3. Surface Parallelism: It checks if two surface are at 180° to each other.

The requirements for the cavity resonator has been shown in figure 2.10.

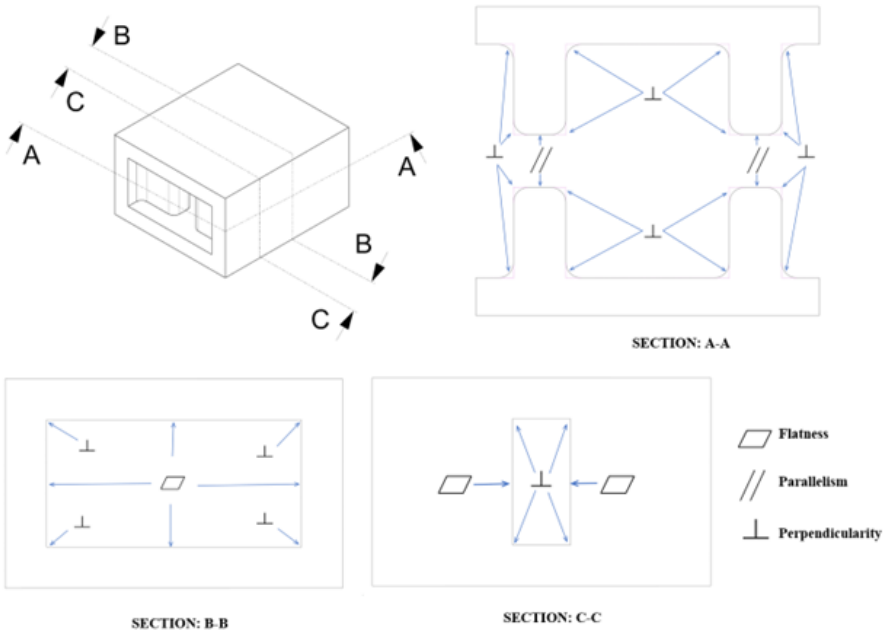

Figure 2.10: Dimensional requirements for the cavity resonator

Surface texture refers to the geometrical irregularities present on a surface. It doesn't include the contribution of form or shape of the surface(Palová et al., 2023).

It consists of the roughness, waviness and lay. The shortest wavelengths surface variations consisting of deviations from actual surface in form of peaks and troughs is referred to as roughness of the part. There are various ways of measuring surface roughness, the most prevalent way in the industry is the arithmetic mean height (R_a). Surface roughness is a geometric property of the surface, and there are no direct methods to measure it(Palová et al., 2023).

The waviness can be explained as surface finish variations which are broadly spaced. The causative agent includes warping from heating and cooling, machining defects from chatter or deflection. It is usually observed over a longer evaluation length and can therefore provide a challenge to measure when the part dimensions are in micro scale(Elder and Elder, 2022).

Lay is the pattern formed on a surface due to the machining operation. It could be parallel, circular, cross hatched or multi directional. In case of additive manufacturing, the printed layers could be counted as the lay(Elder and Elder, 2022).

2.6.1 Factors affecting surface roughness and dimensions

Dimensional deviation and surface roughness is controlled by process dependent factors, material dependent factors, design dependent factors.

Process dependent factors
The orientation of part and where it lies on the printing space can have impact on the accuracy. The position of support structures and the indirect impact of it on the thermal gradient on the part. The layer thickness and binder saturation level could also contribute to the variations. Also, the anisotropic sintering and how it has been compensated has an effect on precision and accuracy of the parts.Thermal Gradients present during the printing, as discussed above, internal residual stress could lead to deformations or warping(Leach and Carmignato, 2020)(Kafara et al., 2018). Smaller layer thickness would give a superior definition of geometry leading to higher dimensional accuracy. In MEX, the wall printing speed also defines both dimensional accuracy and surface roughness. In PBF-L/M systems, like in other processes, finer surface roughness can be obtained by reducing the layer thickness. The laser power and the scanning speed have not so significant influences on the roughness(Cao et al., 2021).

In powder-based systems, the roller mechanism also has an influence over the part properties. The magnitude of applied load, roller material and it's interaction with the powder particles, powder flowability, roller and part interactions, layer shift are other parameters to look into. Inn BJT, binder interactions also play a role. There could be a possibility where the binder fluid flows beyond the intentional boundary reducing surface precision. This is referred as bleeding. A weak binder could lead to poor adhesion compromising part accuracy(Mostafaei et al., 2021).

Material dependent factors
A broader Powder Size Distribution (PSD) could lead to denser powder bed packing. This would lead to a denser powder bed, effectively reducing the shrinkage during sintering. Broader PSD would however lead to an increase in the surface roughness as the possibility of small sized powder to agglomerate also increases. Smaller the particle size, better the surface parameters would be.Powder size distribution, Particle Size, Powder Morphology(Mostafaei et al., 2021).

Design dependent factors
There could be a deterioration of surface due to complex features or interaction of different conditions. One example would be the improvement in perpendicularity of the part with or without the addition of fillets. It has been explained in the results section. Processes using sintering have a chance to undergo defects like sagging and surface cracks due to rapid binder evaporation(Zhao

et al., 2023).

2.6.2 Dimension measuring techniques

This section explains various techniques to measure the dimensions of the resonator.

Optical metrology and digitalization
The use of stripe light projection principle can be used to measure outline or deviation of structures. The usual range of this method is between 2 to 5000mm with a tolerance of 2µm to 650µm(Kafara et al., 2018).

Cordinate Measuring Machine (CMM)
A coordinate measuring machine has been used extensively in the industry for quality assurance and has been a go-to tool for GD&T measurements. There are Laser based CMM machines in the current market which can scan with an accuracy of 3µm, compare the scans with the CAD geometry and provide info on the flatness, perpendicularity, angular, parallelism, coaxiality, symmetry and distance measurements. One of the drawbacks of this method is that it cannot measure hidden geometries as it is based on a stylus(mechanical) or laser(optical) mechanism(Keferstein, 2011).

Computed Tomography (CT) scanning
While the other two mentioned methods are used extensively for exterior surfaces which could be optically or mechanically accessed, CT which is an Non Destructive Test (NDT) opens options to have a dimensional assessment inside a part. Modern CT machines boasts of multiple X-Ray sources and scanners that could possible provide a 3D render of the part(Du Plessis et al., 2018).

2.6.3 Surface Roughness measuring techniques

This section explains various techniques to measure the surface roughness of the resonator.

Mechanical Contact Stylus Technique
This method exploits the coordinate metrology field and uses a stylus with a small contacting force to capture the mechanical surface roughness and convert into electrical signals. These signals are then processed to provide surface profile or areal topography image. As the process is a mechanical contact-based process, there is a high probability to damage the surface during the test depending on the hardness of the scanned surface. Also, the stylus tip size controls the scale of the measurement and is often best for macro level surface readings(Ali, 2012).

Optical Measurement Techniques
Using light is a strong nanometrology tool used in surface characterization.

This method offers advantages like no contact, nondestructive nature of tests, fast measurements. Challenges include surface characteristics like reflectivity, fine surface features that could cause diffraction, and deep valleys that could potentially cause multiple scattering(Ali, 2012).

White light interference microscopy combines the power of nanoscale scanning of interferometers and microscopes which could help scan a remarkable vertical range of up to 1mm. The white light option unlike monochromatic light provides a greater accuracy. Higher magnification scans produce higher resolution images at the cost of a smaller scanner area and vice-versa. Thin film deposition on surface could jeopardize results so it is advised to be mindful of the sample preparation(Ali, 2012).

In confocal optical microscopy, it uses two lenses of same focal point. The confocal microscope incorporates the ideas of point-by-point illumination of the specimen. The out of focus light is rejected. A vertical scanner moves the lens which helps analyze different heights. The differentiation of depth helps generate a scan or image of the surface. Laser microscopes such as VK-X3000 use this method of "confocal principle" to perform precise measurements (*https://www.keyence.com/*).

Non-Optical Measurement Techniques
The optical measurement techniques mentioned above offer a precision in the range of 100nm to 1mm (Ali, 2012). Non optical methods like scanning tunneling microscope (STM) and atomic force microscope(AFM) can provide a finer resolution of upto 1 nm(Ali, 2012).

3

Design of Experiment and Experimental Approach

This section discusses the design of experiment, setup, and the equipment used for the study in detail.

3.1 Design of Experiment (DOE)

The design of experiment involved enlisting the parameters that would impact the dimensional accuracy and the surface finish. The final goal is to achieve the required frequency and Q-factor. The frequency is dependent on the dimensional accuracy and the Q-factor depends on the surface conductivity and roughness of the resonator. The internal surfaces and dimensions are the critical parameters which affects the performance of the resonator (Thanh Do, Personal Communication).
The variables involved were process, orientation, material, frequency, critical surface/face from a surface roughness point of view and dimensional accuracy. In an ideal case, a DOE could be built around these variables. Some of the variables were removed or simplified to make things work in schedule. Considering the variables the full factorial method was chosen to design the experiment(Davim, 2016). Each variables are explained in this sections.

Process
After selection of process suitable for the application, 5 potential suppliers were investigated. Robert Bosch GmbH supported the project by providing their expertise for Binder Jetting. Other potential process were dropped due to timeline contraints thereby removing process as a variable.

Orientation
The orientations were decided to vary the dimensional accuracy and surface roughness in the cavity. The staircase effect observed in Binder Jetting can only be removed using post processing.(Hartmann et al., 2022) Elimination of post processing requires an understanding of how this effect might affect the product's performance. For the ease of part identification, a number deboss was made on the part. A cheat sheet was made to keep track of the parts, which is attached in the appendix A.1.

Orientation Codes	X-Direction	y-Direction	z-Direction
1	0°	0°	0°
2	90°	0°	0°
3	45°	45°	0°
4	0°	90°	0°

Table 3.1: Print orientations for the experiment.

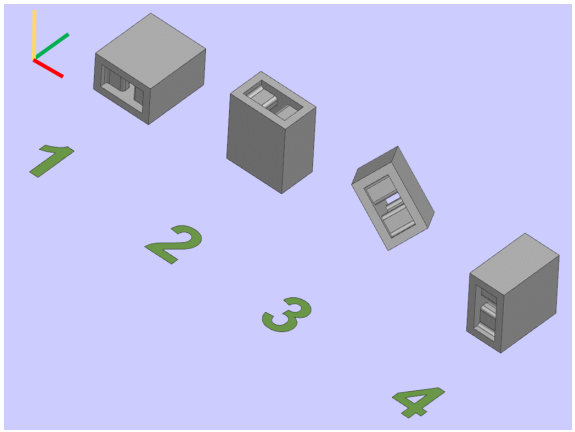

Figure 3.1: Cavity resontators orientations for printing as per table 3.1

The orientations decided as per table 3.1 and figure 3.3 shows a visual representation of these orientations.

Material

The required material properties include materials which have excellent surface roughness and dimensional accuracy for the material used in the part. From an electrical standpoint, materials providing high electrical conductivity is preferable (Torbjorn, Personal Communication). Material was also limited based on the powder loaded in the supplier's printer. There were four candidates for the material. 316L stainless steel (SS), 17-4PH SS, Aluminum and Copper. Copper is the material of choice for it's high electrical conductivity. Due to unavailability and supplier's ease, the first batch of print was made in 316L SS and the second in 17-4PH SS. Qualitatively speaking, 17-4PH SS presents better dimensional accuracy post sintering (Bosch, Personal Communication).

Dimensional Accuracy

The dimensional accuracy directly contributes the value of frequency filtered by the cavity resonator. Each dimensional value adds to the total count of the variables thereby significantly increasing the number of tests required. It was decided to measure the values only for information and check for the opening of the resonator.

Frequency

Three frequencies were selected based on the frequency requirements by Ericsson and to seek the challenge of printing miniscule parts. The 23 GHz although significant in size provides a good contrast in dimension to the other two frequencies and would provide good data on dimensional accuracy as the shrinking effect of sintering would be more pronounced. The 80 and 110 GHz provide a challenge to be manufactured using subtractive manufacturing.

Critical Surface
When it comes to surface roughness, ideally all the inside surfaces of the cavity should be under consideration. From the first batch of prints, it was observed that there are three types of surface behavior. The one kind of surfaces showed similar roughness values and showcased the staircase effect. And the other two are the surfaces which are perpendicular to the powder bed showed a particular value of roughness as well as the layer printed parallel to the bed. So three surfaces were selected and measured the surface roughness.
The process, material, and dimensional accuracy was eliminated as parameters. The remaining variables are four orientation, three frequency and 3 surfaces for surface roughness. This leads to a total of 36 experiments.

After correlating the surface roughness and electrical values, the next batch of parts are to be printed include orientations that are the best performers in the electrical tests. The objective of this batch would be to increase the statistical power of the measurements made ensuring repeatability(Davim, 2016).

3.2 Resonator design and printing

The cavity resonator was designed by Ericsson for 23GHz, 80GHz, and 110GHz according to IEC 60154-2: 2016-2017 using Ansys HFSS (High Frequency Simulator Software) and PTC Creo. The figure 3.2 shows the schematics of the cavity resonator and the table 3.2 shows the dimensions of the resonator.

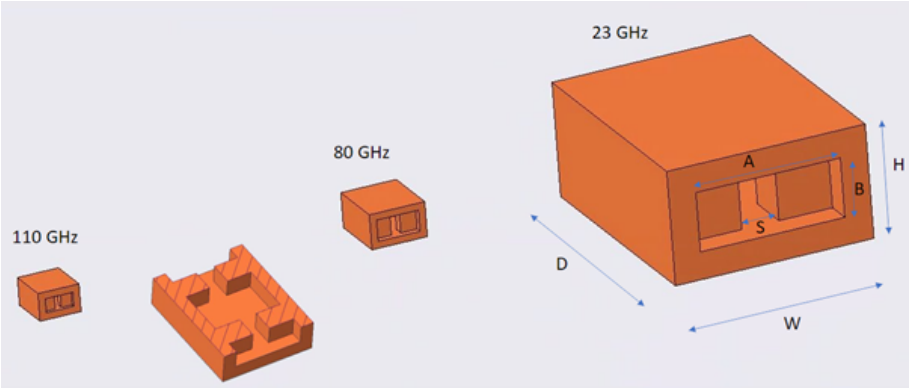

Figure 3.2: Cavity resontators designed for 23GHz, 80GHz, 110GHz

Frequency/Wavelength	W	H	D	S	A	B	WG
23GHz/13	14.668	8.318	18.7	2.74	10.668	4.318	R220
80GHz/3.75	4.1	2.55	4.65	0.7	3.1	1.55	R740
110GHz/2.73	3.032	2.016	3.36	0.45	2.032	1.016	R1200

Table 3.2: Dimensions of the respective resonators. (All dimensions are in mm)

The initial test prints were printed with Markforged PX100™ on stainless steel 316L. All parts were printed in one single orientation, as in the figure 3.3.

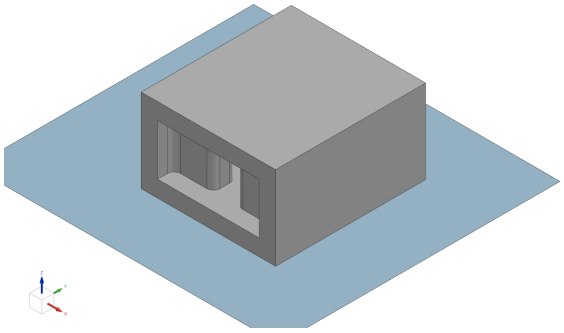

Figure 3.3: Initial Orientation for the first batch printing

The holders were specially designed to hold the resonator between the waveguide flanges for the electrical characterisation. The accuracy of these holders is critical for the measurements, as the resonator should sit firmly in between the flanges to get the output. The holders are printed upright to obtain accurate cavity dimensions. The optimum printing orientation was not chosen because the cavities obtained wasn't accurate.

These are printed using FormLabs Form 3+ VPP technology in the orientation shown in figure 3.4a to get a smooth finish and high dimensional accuracy.

3.3 Electrical Characterization

The electrical characterization was performed using the Vector Network Analyzers (VNA) by Thanh Do and Thomas Emanuelsson at Chalmers and Ericsson facilites.VNA can measure the resonant frequency and the Q-factor of the resonator. The figure 3.5 shows the basic working idea of a VNA. VNAs are used to validate the results from the simulation.

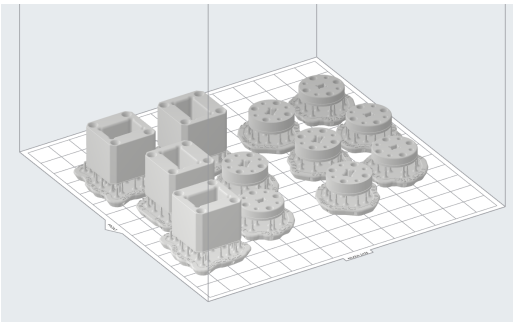

(a) Print bed of Form 3+ containing holders

(b) 80GHz Holder in between the E-band waveguides

Figure 3.4: Waveguide holders printed using VPP for precise alignment between waveguides

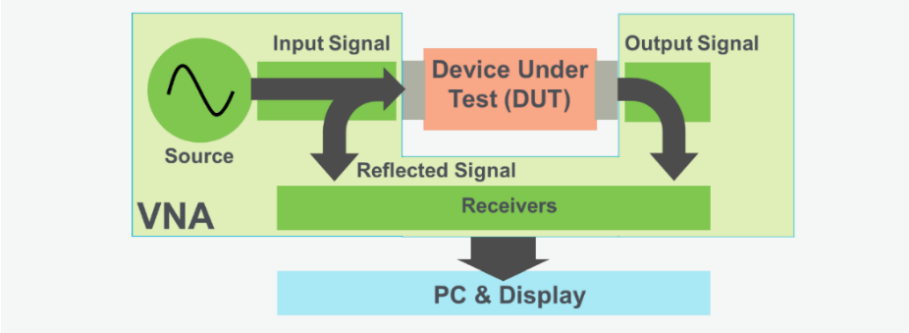

Figure 3.5: Simplified schematic of a VNA. Taken from (VNA, 2024)

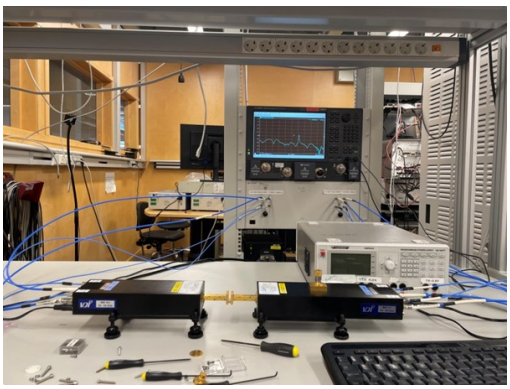

(a) VNA test setup at Chalmers for E-band and F-band

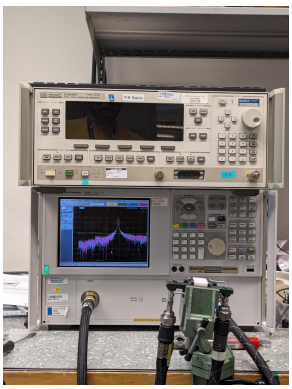

(b) VNA test setup at Ericsson for 23GHz

Figure 3.6: Electrical characterization VNA test setup

Virginia Diodes VDI frequency extenders (The two black box seen in the fig-

ure 3.6a) are used in the test setup to extend the frequency from the E-band (60-90GHz) to F-band (90-140GHz). The reference plane for the F-band test is calibrated according to the frequency extenders flanges. The simulation of the electrical tests were done on Ansys HFSS. The results from simulation are used to compare the results from the experiments.

3.4 Dimensions and Surface Characterization

The external dimensions could be measured using a vernier caliper. With the available resources, the internal dimensional accuracy can be measured in two ways. One involves a non-destructive approach using X-ray computed tomography (XCT). XCT was used to take images of the cavities and then measure the internal dimensions. The XCT available had a single point focus, which results in blurry focus away from the point of focus. This effect could be seen in fig 3.7a

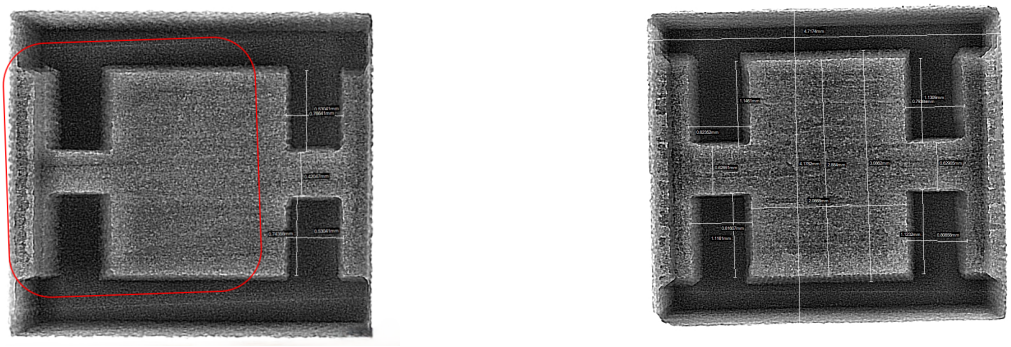

(a) Loss of focus observed in the red box when focusing on the structure on right

(b) XCT image of a 80GHz resonator with internal measurements

Figure 3.7: XCT images of 80GHz

The other method is to section the parts and measure the internal dimensions using a stereo microscope. 23GHz was cut using an IsoMet high-speed precision cutter with a 0.5mm thick aluminum oxide blade. 80GHz and 110GHz are difficult to cut through. Grinding operation is performed to get to the internal cavities. A grit size of 800 is used to avoid smearing of the edges. The distortion issue from the XCT was solved with this method.

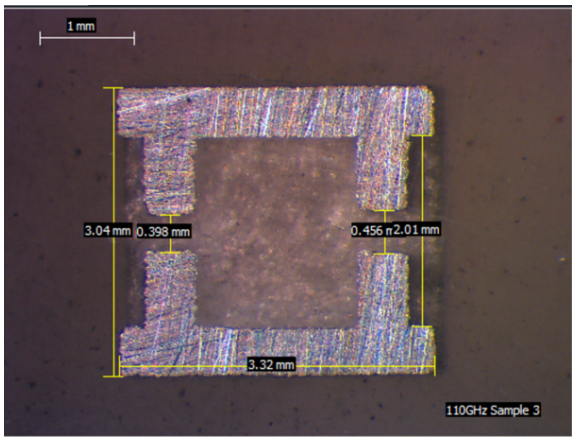

Figure 3.8: Stereo microscope image of a 110GHz resonator with internal measurments after sectioning

The surface roughness test was performed using two different methods. Optical profile interferometer at Chalmers was used to evaluate the surface roughness of the resonator. It is an optical method which uses multiple light sources to combine data to make precise measurements to obtain surface roughness, topography and profile. R_A values are used to characterize the surface roughness of the specimen.The figure 3.9 shows the 3D scan result of the external surface of the resonator.

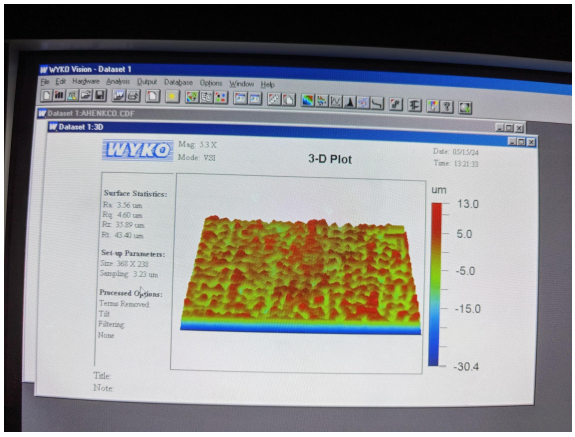

Figure 3.9: Image depicting the 3D scan capabilities of Optical Profile Interferometer at Chalmers

Reflecting light from the surface can hinder the measurements of the interferometer. This challenge was overcome by using a 3D laser scanning microscope. It was used to perform the scan to evaluate the surface roughness by using a white light-laser interferometry to eliminate the reflection and get accurate results. The Ericsson facility at Borås has the Keyence VK-3000 3D laser microscope, which can perform high resolution surface characterizations.

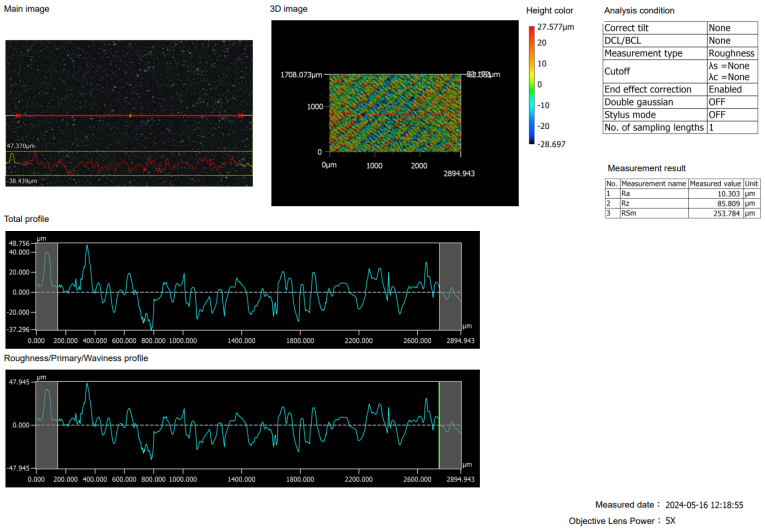

Figure 3.10: Image depicting the surface roughness characterization of the 3D laser Microscope at Ericsson

Figure 3.10 provides information about the R_A, R_Z, and R_{Sm} value across the horizontal line. It also provides a 2D representation of the surface profile across the line. This information is vital for understanding the print layers.

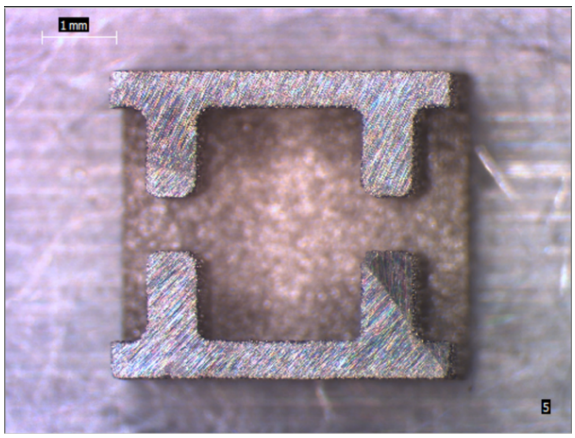

Figure 3.11: Section of the 80GHz Resonator with fillets

Analysing the Data from the first batch of prints, a design (figure 3.11) change was proposed to incorporate fillets, to get a better control over the surfaces. The hypothesis was that since in BJT, the binder being dropped would be spherical in nature, a round perimeter would be easier to control. This new design was also done by Ericsson using Ansys HFSS and PTC Creo.

4

Results and Discussion

This section describes the results from electrical and surface characterizations and its analysis of the printed resonators.

4.1 Electrical Characterization

As mentioned in the section 3.3, the tests are done on VNA. The electrical tests done on the first batch of prints for 23 GHz failed to produce a strong resonant frequency. The output dB was very low as seen in the figure 4.1a compared to the simulation, which is shown in the figure 4.1b.

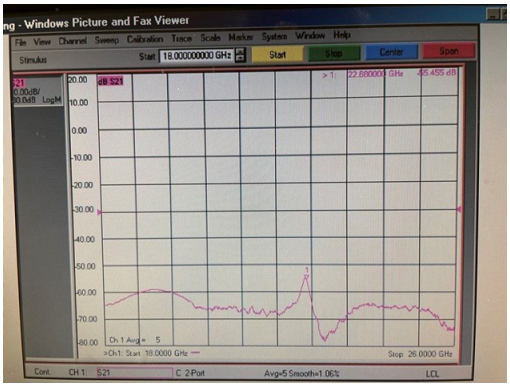

(a) 23GHz failed electrical Characterisation

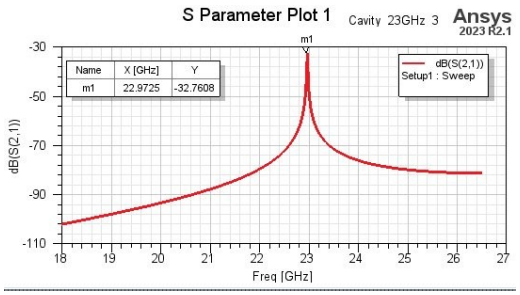

(b) 23GHz (Without fillets) electrical simulation

Figure 4.1: 23GHz simulated electrical Characterization

The reason for the failed test is unknown, It might correspond to defects in the resonator or issues in the test setup. Further investigations would be required for a conclusion. The investigation was not completed due to the limited number of printed parts.

The VNA tests for the first print 80GHz and 110GHz produced resonant frequency close to the simulated frequency. The experimental Q-factor is lower than the simulated Q-factor. This can be due to loose connection with the waveguides during tests, dimensional accuracy, surface roughness, or can be a

combined result of the mentioned factors.

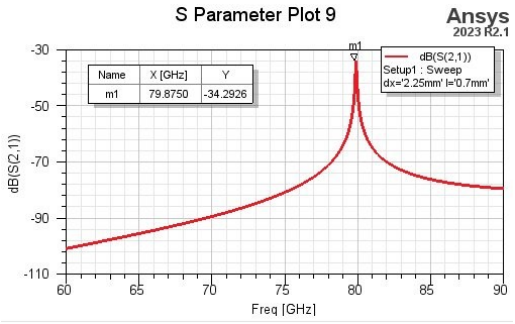

(a) 80GHz (Without fillets) simulated electrical result

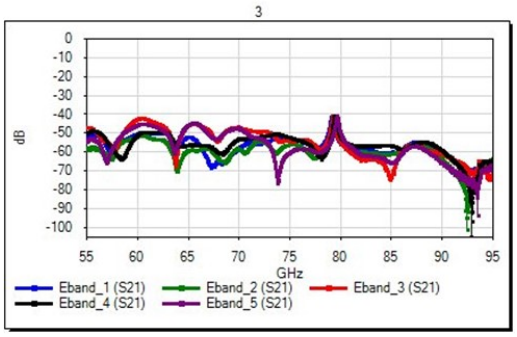

(b) 80GHz (Without fillets) measured results

Figure 4.2: 80GHz simulated and experimental electrical Characterization

The figure 4.2a shows the simulated frequency of 80GHz. The value is 79.8750 GHz with a Q-factor of 304 for stainless steel considering the surface roughness R_A equal to 10µm. Figure 4.2b shows the experimental results of all 80GHz specimens. The frequency peak is close to 80GHz with an average value of 79.31GHz with an average Q-factor of 311. The table 4.1 shows the resonant frequencies of all samples involved in the test. The experimental Q-factor showed in the table 4.1 is on par to the simulated value.

Sample	F_{res} (GHz)	**Q**
1	79.1	287
2	79.275	288
3	79.2	344
4	79.35	318
5	79.625	318.5

Table 4.1: Resonant frequency and Q-factor of 80GHz resonators without fillets

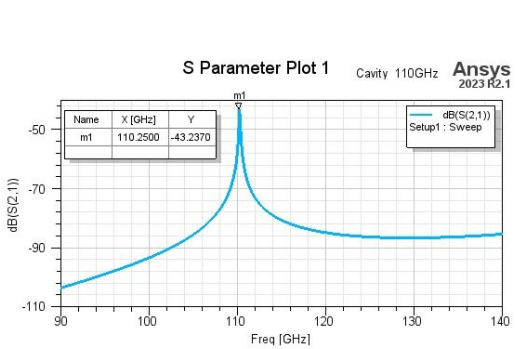

(a) 110GHz (Without fillets) electrical simulation

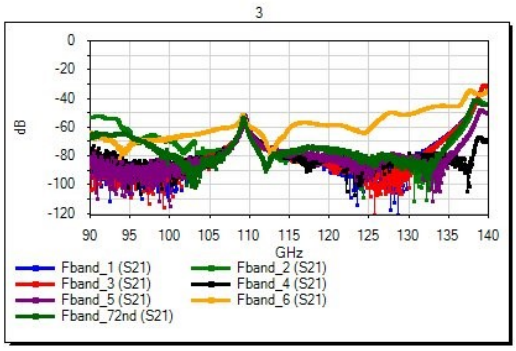

(b) 110GHz (Without fillets) measured results

Figure 4.3: 110GHz simulated and experimental electrical Characterization

Similarly, the figure 4.3a shows the simulation of 110GHz resonator. The simulated frequency is 110.25GHz with a Q factor of 292. The table 4.2 and the figure 4.3b shows the experimental results for 110GHz. The 110GHz resonators also produced a similar result to the 80GHz regarding the resonant frequency and the Q-factor. The only anomaly was with yellow line or sample 6 in figure 4.3b, possibly due to loose connection between the flanges during the test.

Sample	F_{res} **(GHz)**	**Q**
1	109.25	292
2	109.313	291
3	109.25	292
4	109.313	308
5	109.438	304
6	109.094	218
7	109.188	303

Table 4.2: Resonant frequency and Q-factor of 110GHz resonators without fillets

The proposed design changes to add the fillets have brought changes in the results as well. The tests done on 23GHz with the fillets have yielded comparative results compared to the non-filleted one. A new simulation was done with the changes in design to find the expected resonant frequency and Q-factor.

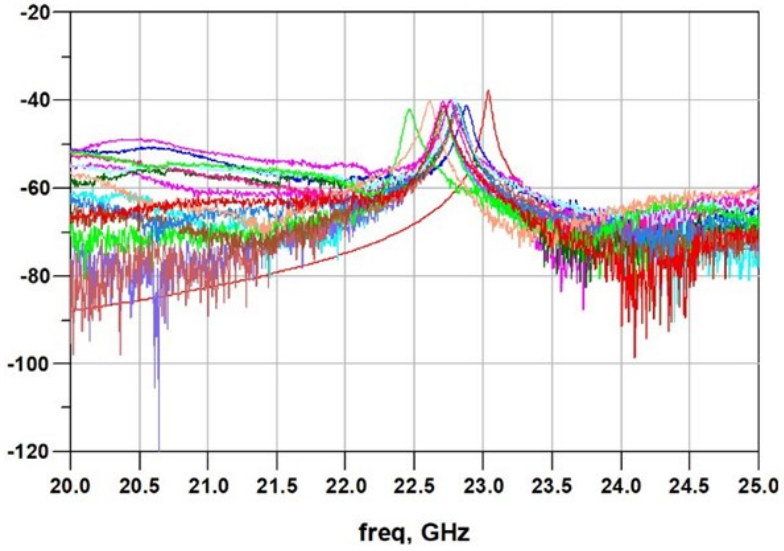

Figure 4.4: 23GHz(with fillets) simulated electrical characterization along with the experimented results

Sample	F_{res} (GHz)	**Q**
Batch 9_1	22.87	325
Batch 9_2	22.71	324
Batch 9_3	22.465	321
Batch 9_4	22.61	290
Batch 10_1	22.72	330
Batch 10_2	22.72	325
Batch 10_3	22.71	325
Batch 10_4	22.71	284
Batch 11_1	22.8	326
Batch 11_2	22.8	326
Batch 11_3	22.8	304
Batch 12_1	22.76	305
Batch 12_2	22.765	285
Batch 12_3	22.81	304
Batch 12_4	22.79	304

Table 4.3: Resonant frequency and Q-factor of 23GHz resonators with fillet

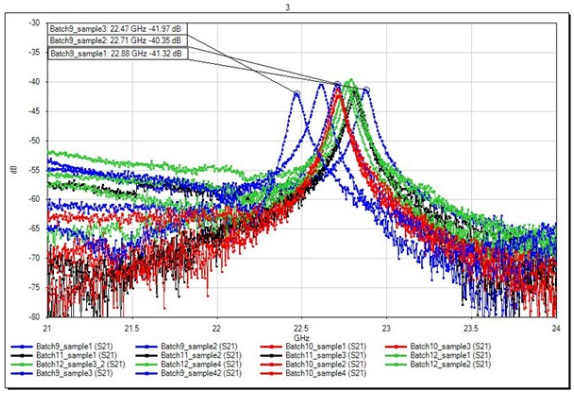

Figure 4.5: 23GHz(with fillets) electrical characterization

The figure 4.4 shows the new simulated frequency along with the test results. The new simulated q factor comes around 600. The table 4.3 shows the experimental results of the 23GHz with the fillets. The figure 4.5 shows the graph between resonant frequency and the output power of all the test specimens. In the graph each color indicates different orientations. The resonant frequency was fluctuating for each orientations. The shift in the resonant frequency from the simulation can be due to the dimensional inaccuracy happened during the printing. Specimen 9 (The blue color in figure 4.5) shows the most fluctuating in the resonant frequency. This can be seen as an anomaly as it wasn't seen on other samples. Another reason for the shift in resonant frequency can be dimensional inaccuracy after incorporating the fillets into the design. As in the figure 4.6, the walls are not parallel, which can cause a shift in the frequency. Another possibility for the shift in frequency can be the result of the 'elephant foot' effect observed during the printing process. Batch 10 and 11 showed good repeatability in resonant frequency with batch 11 being close to the design frequency. Batch 12 showed better power output compared to others.

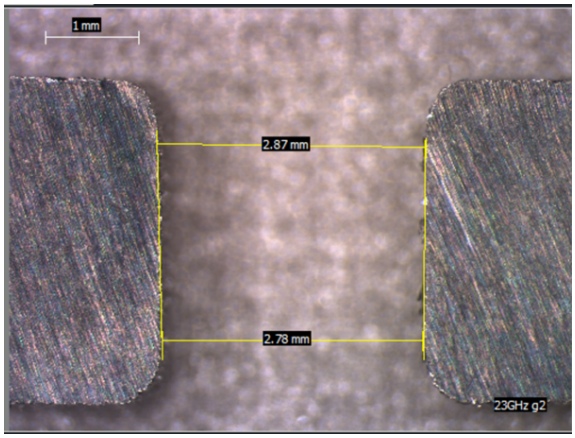

Figure 4.6: 23GHz(with fillets) gate dimension measurement

The Q factor of 23GHz was also less than the simulated Q factor. It can be because

Sample	F_{res}	Q
Batch 5_ 1	77.83	325
Batch 5_ 2	77.58	353
Batch 5_ 3	77.91	346
Batch 5_ 4	77.64	310
Batch 6_ 1	77.01	350
Batch 6_ 2	77.53	325
Batch 6_ 3	77.7	324
Batch 6_ 4	77.91	312
Batch 7_ 1	76.65	320
Batch 7_ 2	77.12	302
Batch 7_ 3	76.72	295
Batch 7_ 4	76.42	355
Batch 8_ 1	77.1	342
Batch 8_ 2	77.06	342
Batch 8_ 3	77.1	321
Batch 8_ 4	76.56	306

Table 4.4: Resonant frequency and Q-factor of 80GHz resonators with fillets.

Sample	F_{res}	Q
Batch 1_ 1	105.7	265
Batch 1_ 2	105.8	265
Batch 1_ 3	105.1	263
Batch 1_ 4	105.4	351
Batch 2_ 1	104.4	261
Batch 2_ 2	104.8	262
Batch 2_ 3	104.2	261
Batch 2_ 4	105.7	264
Batch 3_ 1	105.7	264
Batch 3_ 2	105.2	234
Batch 3_ 3	105.3	263
Batch 3_ 4	106.2	354
Batch 4_ 1	106.3	266
Batch 4_ 2	106.1	265
Batch 4_ 3	106.2	354
Batch 4_ 4	106.3	266

Table 4.5: Resonant frequency and Q-factor of 110GHz resonators with fillets.

Table 4.6: 80 and 110GHz electrical Characterization tables

of the same reasons as the non-filleted ones. The 80 and 110GHz resonators with fillets exhibited a better Q-factor than the resonators without fillets. The table 4.4 shows the Q-factor and the resonant frequency of the 80GHz and the table shows 4.5 of the 110GHz. Both 80GHz and 110GHz showed a shift in the resonant frequency from the simulated frequency. The shift observed is a significant shift when compared to the resonators without fillets. The exact reason for the large frequency shift is unclear. Batch 5 and Batch 6 were the ones with least deviation from the designed frequency. The deviation among the batches are in the range of 300-400MHz for the 80GHz and 500MHz-1.5GHz for 110GHz. The shift in the designed frequency can be associated with the dimension inaccuracies, although the design changes made to incorporate the fillets were compensated, the huge shift in the frequency were not expected.

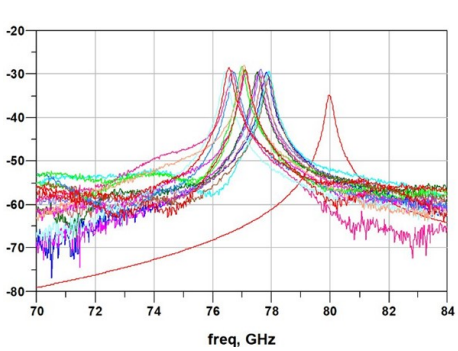

(a) 80GHz(with fillets) electrical Characterization

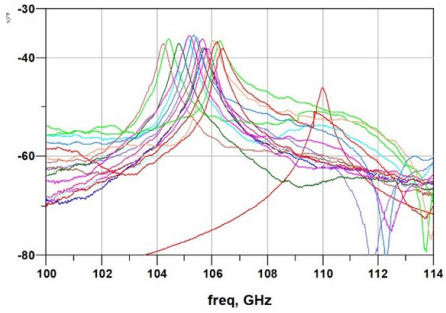

(b) 110GHz(with fillets) electrical Characterization

Figure 4.7: 80GHz and 110GHz electrical Characterization graphs

The power output for the new 80 and 110GHz were higher than the simulation. This can be seen in the figures 4.7a and 4.7b. This might be due to better vertical surfaces achieved by adding the fillets. This better power output is also reflected in getting better Q-factor than the simulated value for some specimens.

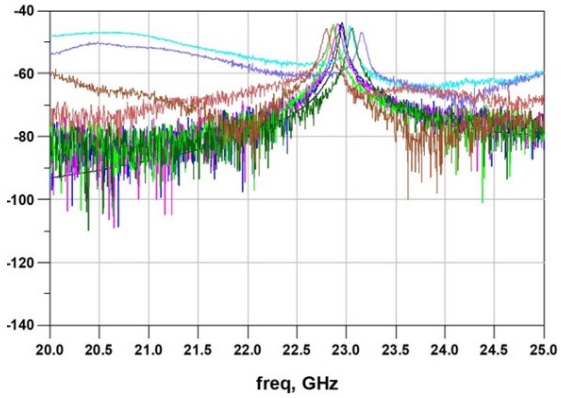

Figure 4.8: 23GHz (MJT) electrical characterization

Initial design without the fillets was used for the manufacturing of resonators using MJT. The 23 GHz was performing very close to the designed frequency and q factor. The 23GHz was designed to resonate at 22.92GHz, batch 21 was exactly giving out 23GHz as seen in the table 4.7. The figure 4.8 shows the simulated graph of the MJT manufactured resonators. All the orientation specimens were performing very close to the design frequency of 22.9GHz.

Batch	F_{res} (GHz)	Q
Batch 21_1	22.91	458
Batch 21_2	22.94	417
Batch 22_1	23.04	460
Batch 22_2	23.16	421
Batch 23_1	22.87	416
Batch 23_2	23.06	420
Batch 24_1	22.86	457
Batch 24_2	22.8	456

Table 4.7: 23GHz (MJT) electrical characterization

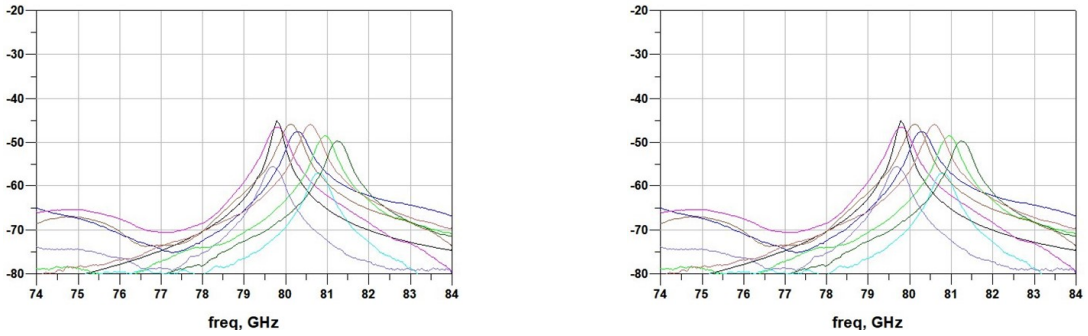

(a) 80GHz (MJT) electrical characterization

(b) 110GHz (MJT) electrical characterization

Figure 4.9: 80GHz and 110GHz electrical Characterization graphs

The batch 17 of the 80GHz reproduced the exact design frequency. Other orientations as seen in the table4.8 are also very close to the design frequency, with a deviation under 500MHz. The batch 19 and 20 produced resonant frequency greater than the design frequency. The q factor is on the lower side compared to the BJT which was unexpected, as theoretically MJT has better surface finish. This could be due to the undissolved support material stuck inside. This can also be the reason for higher resonant frequency as the stuck supports reduces the overall volume of the cavity.
110GHz also showed a similar results. One of the specimen of batch 14 failed in the test without giving any results as seen the table 4.9.Batch 13 was producing resonant frequency as same as the design frequency. Rest of the orientations were producing around 1-1.5GHz higher than the design frequency. The reasons may be similar to the 80GHz, support material stuck inside. Figure **??** shows the positive shift from the designed 110GHz.

batch	F_{res} (GHz)	Q
batch 17_1	80.29	183
batch 17_2	79.8	170
batch 18_1	80.79	172
batch 18_2	79.69	170
batch 19_1	80.94	186
batch 19_2	81.26	189
batch 20_1	80.59	179
batch 20_2	80.12	184

Table 4.8: 80GHz (MJT) electrical characterization

batch	F_{res} (GHz)	Q
batch 13_1	110.00	220
batch 13_2	110.20	220
batch 14_1	x	x
batch 14_2	111.30	223
batch 15_1	111.70	224
batch 15_2	111.80	224
batch 16_1	111.10	222
batch 16_2	110.60	222

Table 4.9: 110GHz (MJT) electrical characterization

Table 4.10: 80 and 110GHz MJT electrical Characterization tables

4.2 Dimension measurements

The dimensional accuracy is critical for the resonator to produce the designed resonant frequency.

	x (o)	*x (u)*	*y (o)*	*y (u)*	*z*	*x (o-u)*	*y (o-u)*
23GHz_9_1	-18,86	-18,8	-15,11	-14,88	-8,48	0,06	0,23
23GHz_9_2	-18,69	-18,62	-14,88	-14,88	-8,40	0,07	0
23GHz_9_3	-18,93	-18,62	-15,11	-14,87	-8,47	0,31	0,24
23GHz_10_1	-18,74	-18,69	-14,77	-14,77	-8,38	0,05	0
23GHz_10_2	-18,69	-18,66	-14,76	-14,72	-8,34	0,03	0,04
23GHz_10_3	-18,71	-18,68	-14,84	-14,82	-8,35	0,03	0,02
23GHz_11_1	-18,62	-18,57	-14,79	-14,76	-8,34	0,05	0,03
23GHz_11_2	-18,75	-18,66	-14,93	-14,82	-8,39	0,09	0,11
23GHz_11_3	-18,59	-18,54	-14,78	-14,75	-8,32	0,05	0,03
23GHz_12_1	-18,51	-18,45	-14,80	-14,76	-8,36	0,06	0,04
23GHz_12_2	-18,56	-18,51	-14,87	-14,80	-8,38	0,05	0,07
23GHz_12_3	-18,58	-18,52	-14,85	-14,79	-8,36	0,06	0,06

Table 4.11: 'Elephant foot' effect data

The table 4.11 shows the data for the external dimensions and the deviations of the 23GHz. *x (o)* is the length of the resonator on bottom side, and *x (u)* is the length of the similar edge on the top side during sintering. Similarly in the y-direction *y (o)* and *y (u)*. The difference in the dimensions are visible here. This deviation can be a result of the anisotropic shrinkage of the part during the sintering process. The 'elephant foot' effect is more prominent in the 23GHz.
The 'elephant foot' effect is not visible in the 80GHz and 110GHz resonators. The deviations from the CAD dimensions is also less when compared to the deviations happened in 23GHz. It is observed that the deviations from the CAD dimensions

are more prominent when the size of the resonator increases.

4.3 Surface Roughness Measurements

Three main surface profile was identified and discussed in section 3.1. The line surface roughness was measured of these surfaces. The detailed data for the three surfaces from four different orientation of the 110GHz BJT is in the appendix B. The surface roughness of BJT produced resonators are in the range of 5-11μm. Changing the surface roughness didn't brought any significant change in the q factor. Different orientations did not brought any changes in the performance. The study couldn't find any recurring patterns or significant change in performance with different surface roughness.

The surface of the MJT part couldn't be calculated as the parts was received very late for surface characterisation. From the supplier's communication, the average line surface roughness is around 3-5μm.

5

Conclusion & Future Studies

The idea of this thesis was to identify a suitable process to manufacture cavity resonators, especially in the case where the size becomes too small to manufacture them conventionally. Another goal was to study the behavior of output frequency and quality factor when the orientation of the part is varied, which in turn changes the dimensional accuracy and the surface roughness of the internal cavity.

Among all the AM processes mentioned, the best fit for this type of application would be BJT, MJT and VPP without much use of post processing. PBF-L/M would also be a good choice, but will require the need for supports. These supports may or may not be efficiently removed by using a postprocessing depending on the complication of the geometry, therefore each design must be carefully evaluated for feasibility. BJT, MJT and VPP will have a secondary step of sintering which results into shrinkage of part and the shrinkage rate would depend on the binder to metal ratio of the green part. This is controlled by parameters such as powder morphology, particle size distribution, binder type, and much more. The better the shrinkage control or at least the understanding of the behavior of the shrinkage the better the dimensional accuracy resulting in achieving the right frequency. Theoretically, VPP provides a superior surface finish followed closely by MJT and then by BJT and PBF-L/M. Good surface finish results in better quality factor. Considering all these requirements and the fact that the potential materials for all these processes include the desired material of copper (because of the requirement of high electrical conductivity), all three processes, MJT, BJT and VPP, would be an optimal choice. One must be mindful of other factors that might affect this choice based on a different situation. Some of these criteria include the possibility of scaling, cost, requirement of multi-material print, possibility of avoiding interaction with loose powder etc. PBF-L/M with postprocessing like hritization could be another possible approach but wasn't investigated further because avoiding postprocessing was one of the parameters of the thesis.

When it comes to electrical performance, for the BJT parts without fillets, there was no response for the 23GHz, and the average frequency came out to be 79.31GHz for the 80GHz and 109.26GHz for the 110GHz. The average Q-factor for 80GHz and 110GHz were 311.1 and 109.26 respectively. According to Ericsson's communication, the variation of Q factor is pronounced when the variation is in the range of 100 s and could be significantly increased by changing to a material of higher conductivity. In all the cases, the Q factor was not varying to that extent, indicating that surface roughness requirements might not be that sensitive. The sensitivity to the

factors was seen to increase as the frequency requirement of the part went higher. There was no observable pattern between the different frequencies printed in the same orientation. For example, the part printed in orientation 3 showed consistency between similar prints for 23 GHz but not so for the 80 and 110 GHz.

With regard to mechanical results, the measurement of the cavity dimensional accuracy seems like a daunting task when there are multiple measurements to be made. Also, the errors would stack up significantly. One way to work around it would be to perform a 3D CT scan followed by geometrical comparison in a CAD environment. When sectioning parts for measuring internal dimensions, several errors like parallelism of cut, smearing of cut surface, operator skills, etc. could play a role in making the readings untrustworthy.

It is rather unclear that how much the surface roughness variation contributes to the Q-factor. For BJT, 3 types of surfaces were identified. One was parallel to the bed when the binder touched the powder, the second was again parallel to the bed but on top of a powder layer spread over an already bound layer. The third type of surface was perpendicular to the bed. The first two types had roughness values quite close to each other with the 2nd type having slightly finer finish. The third surface showed the presence of layers and was rougher than the previous two. Some results were not repeatable for the same orientation and batch. Therefore, having a large sample volume would be effective if productivity and repeatability had to be checked.

The MJT parts showed excellent dimensional accuracy and did well with sharp corners. For the electrical results, it was interesting to see that the average frequencies recorded were on the higher side than the ideal frequency. This indicates that the actual cavity volume was lower than that of the simulated cavity volume. The possible reasons could be inaccurate sintering, or the scaling of the part done for the sintering. On sectioning the part, some left over support material was also found, which could also contribute to the decreased volume. Although the MJT parts had a better surface finish compared to BJT, the Q factor was significantly lower than the expected trend. The left-over support could be one of the reasons for the drop in Q-factor. One future work could be to measure this surface area of this left over support zone and checking for patterns with relation to the Q-factor.

Some of the future work that could be carried out after this thesis includes looking into post-processing to improve the performance. The cavity designs in the market are designed around the conventional subtractive manufacturing, therefore looking at the design from the 'Design for AM' point of view could be exciting. Rather than going for a full metal filter, the part could be printed in polymer and coated with a conductive metal. As mentioned, copper being the choice material, material-related challenges could be interesting directions to investigate.

Overall, this project was a good entry to understand the interaction between AM and the electrical and mechanical performance of a unit cell of a cavity filter.

Bibliography

(2024). What are vector network analyzers | VNAs explained.

Ali, S. H. R. (2012). Advanced nanomeasuring techniques for surface characterization. *ISRN optics*, 2012:1–23.

Beevers, E., Neumayer, D., Bonvoisin, B., Brandão, A., Hansal, S., Doppler, M., Rohr, T., and Van Hooreweder, B. (2024). Effect of Hirtisation treatment on surface quality and mechanical properties of AlSi10Mg samples produced by laser powder bed fusion. *Materials today communications*, 38:108042.

Cao, L., Li, J., Hu, J., Liu, H., Wu, Y., and Zhou, Q. (2021). Optimization of surface roughness and dimensional accuracy in LPBF additive manufacturing. *Optics laser technology/Optics and Laser Technology*, 142:107246.

Cui, Z. (2008). *LIGA. In: Li, D. (eds) Encyclopedia of Microfluidics and Nanofluidics*, pages 1000–1003. Springer US, Boston, MA.

Davim, J. P. (2016). *Design of experiments in production engineering*.

Du Plessis, A., Yadroitsev, I., Yadroitsava, I., and Roux, S. G. L. (2018). X-Ray Microcomputed Tomography in Additive Manufacturing: A review of the current technology and applications. *3D printing and additive manufacturing*, 5(3):227–247.

Elder, S. and Elder, S. (2022). The Basics of Surface finish | GDT Basics.

Ericsson (2021). 5G by Ericsson. Retrieved January 27, 2024, from http://www.ericsson.com/49f1c9/assets/local/5g/documents/07052021-ericsson-this-is-5g.pdf .

Ericsson (n.da). Microwave, retrieved january 27, 2024, from https://www.ericsson.com/en/porfolio/networks/ericsson-radio-system/mobile-transport/microwave.

Ericsson (n.db). Our purpose, vision and values. retrieved january 27, 2024, from https://www.ericsson.com/en/about-us/our-purpose.

Eßbach, C., Fischer, D., and Nickel, D. (2021). Challenges in electroplating of additive manufactured ABS plastics. *Journal of manufacturing processes*, 68:1378–1386.

Faisal, N., Zindani, D., Kumar, K., and Bhowmik, S. (2018). Laser Micromachining of Engineering Materials—A Review. *Materials forming, machining and tribology*, pages 121–136.

Gibson, I., Rosen, D., Stucker, B., and Khorasani, M. (2020). *Binder Jetting*.

Gibson, I., Rosen, D., Stucker, B., and Khorasani, M. (2021). *Additive Manufacturing Technologies*.

Gold, G. and Helmreich, K. (2017). A physical surface roughness model and its appli-

cations. *IEEE transactions on microwave theory and techniques*, 65(10):3720–3732.

Hartmann, C., Van Den Bosch, L., Spiegel, J., Rumschöttel, D., and Günther, D. (2022). Removal of Stair-Step effects in binder jetting additive manufacturing using grayscale and Dithering-Based droplet distribution. *Materials*, 15(11):3798.

Kafara, M., Kemnitzer, J., Westermann, H.-h., and Steinhilper, R. (2018). Influence of binder quantity on dimensional accuracy and resilience in 3D-Printing. *Procedia manufacturing*, 21:638–646.

Keferstein, C. (2011). Fertigungsmesstechnik-praxisorientierte grundlagen, moderne messverfahren.(dimensional metrology–practice oriented basics and modern technologies).

Khan, Q. M. and Kuylenstierna, D. (2024). Analysis of Q-factor for AM-SLM Cavity based Resonators using Surface Roughness Models. *IEEE journal on multiscale and multiphysics computational techniques*, 9:75–83.

Laermer, F., Franssila, S., Sainiemi, L., and Kolari, K. (2020). *Deep reactive ion etching*.

Leach, R. and Carmignato, S. (2020). *Precision Metal Additive manufacturing*.

Lieberwirth, N. C., Harder, N. A., and Seitz, N. H. (2017). Extrusion based additive manufacturing of metal parts. *Journal of mechanics engineering and automation*, 7(2).

Malekabadi, A. and Paoloni, C. (2016). UV-LIGA microfabrication process for subterahertz waveguides utilizing multiple layered SU-8 photoresist. *Journal of micromechanics and microengineering*, 26(9):095010.

Maleki, E., Bagherifard, S., Bandini, M., and Guagliano, M. (2021). Surface post-treatments for metal additive manufacturing: Progress, challenges, and opportunities. *Additive manufacturing*, 37:101619.

Mostafaei, A., Elliott, A. M., Barnes, J. E., Li, F., Tan, W., Cramer, C. L., Nandwana, P., and Chmielus, M. (2021). Binder jet 3D printing—Process parameters, materials, properties, modeling, and challenges. *Progress in Materials Science/Progress in materials science*, 119:100707.

Palová, K., Kelemenová, T., and Kelemen, M. (2023). Measuring procedures for evaluating the surface roughness of machined parts. *Applied sciences*, 13(16):9385.

Paschotta, R. (2007). Q factor. RP Photonics Encyclopedia. Available online at `https://www.rp-photonics.com/q_factor.html`.

RF, E. (2022). What are cavity filters? - everything rf. (n.d.). retrieved may 6, 2024, from https://www.everythingrf.com/community/what-are-cavity-filters.

RISE (2022). Ericsson looking to move from research to production | rise. (n.d.). retrieved from https://www.ri.se/en/our-stories/ericsson-looking-to-move-from-research-to-production.

Sahu, A. K., Malhotra, J., and Jha, S. (2022). Laser-based hybrid micromachining processes: A review. *Optics laser technology/Optics and Laser Technology*, 146:107554.

Shukla, S., Gomathi, N., and George, R. (2014). Autocatalytic silver-plating of aluminium radio frequency waveguides with autocatalytic nickel as the undercoat for space applications. *Surface topography*, 2(4):045004.

Simonovic, A., Rohwer, E., and Stander, T. (2022). Preliminary investigation into the use of silver seed layers in copper electroplating of waveguide parts. *2022 International Conference on Electromagnetics in Advanced Applications (ICEAA)*.

Turner, B. N. and Gold, S. A. (2015). A review of melt extrusion additive manufacturing processes: II. Materials, dimensional accuracy, and surface roughness. *Rapid prototyping journal*, 21(3):250–261.

Zhang, B. and Zirath, H. (2016). Metallic 3-d printed rectangular waveguides for millimeter-wave applications. *IEEE Transactions on Components, Packaging and Manufacturing Technology*, 6(5):796–804.

Zhao, K., Su, Z., Ye, Z., Cao, W., Pang, J., Wang, X., Wang, Z., Xu, X., and Zhu, J. (2023). Review of the types, formation mechanisms, effects, and elimination methods of binder jetting 3D-printing defects. *Journal of materials research and technology/Journal of Materials Research and Technology*, 27:5449–5469.

A

Appendix 1

The table A.1 shows the code debossed on all of the specimens printed to identify them for characterisation.

No.	Frequency(GHz)	Deboss	Qty	Process	Material	Orientation	Supplier
1	110	1	4	BJT	316L	1	Bosch
2	110	2	4	BJT	316L	2	Bosch
3	110	3	4	BJT	316L	3	Bosch
4	110	4	4	BJT	316L	4	Bosch
5	80	5	4	BJT	316L	1	Bosch
6	80	6	4	BJT	316L	2	Bosch
7	80	7	4	BJT	316L	3	Bosch
8	80	8	4	BJT	316L	4	Bosch
9	23	9	4	BJT	316L	1	Bosch
10	23	10	4	BJT	316L	2	Bosch
11	23	11	4	BJT	316L	3	Bosch
12	23	12	4	BJT	316L	4	Bosch
13	110	13	2	MJT	316L	1	XJET
14	110	14	2	MJT	316L	2	XJET
15	110	15	2	MJT	316L	3	XJET
16	110	16	2	MJT	316L	4	XJET
17	80	17	2	MJT	316L	1	XJET
18	80	18	2	MJT	316L	2	XJET
19	80	19	2	MJT	316L	3	XJET
20	80	20	2	MJT	316L	4	XJET
21	23	21	2	MJT	316L	1	XJET
22	23	22	2	MJT	316L	2	XJET
23	23	23	2	MJT	316L	3	XJET
24	23	24	2	MJT	316L	4	XJET

Table A.1: Numbering method followed to identify the different specimens

Orientation Codes	X-Direction	y-Direction	z-Direction
1	0°	0°	0°
2	90°	0°	0°
3	45°	45°	0°
4	0°	90°	0°

Table A.2: Print orientations for the experiment.

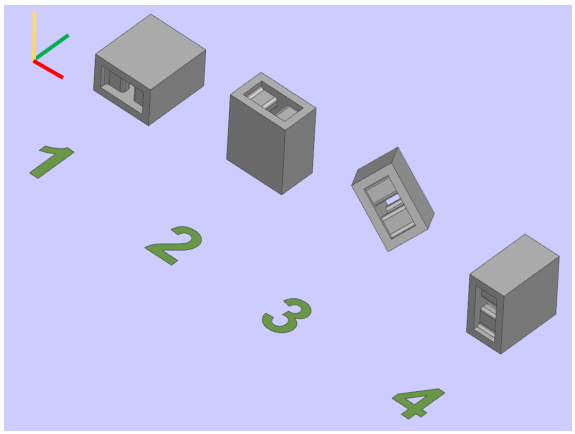

Figure A.1: Cavity resontators orientations for printing as per table A.2

B

Appendix 2

The Appendix B has the surface roughness results of the 110GHz.

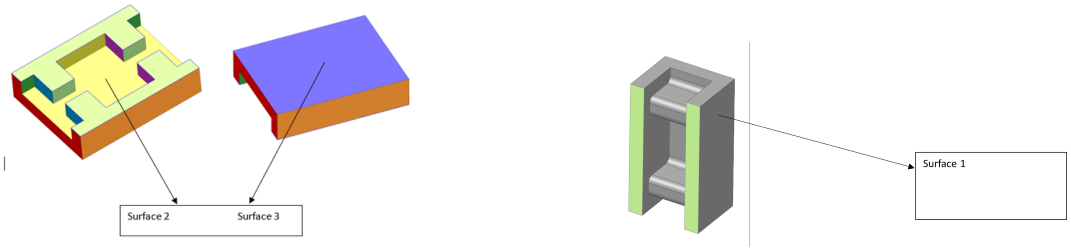

Figure B.1: Different surfaces for surface roughness characterisation

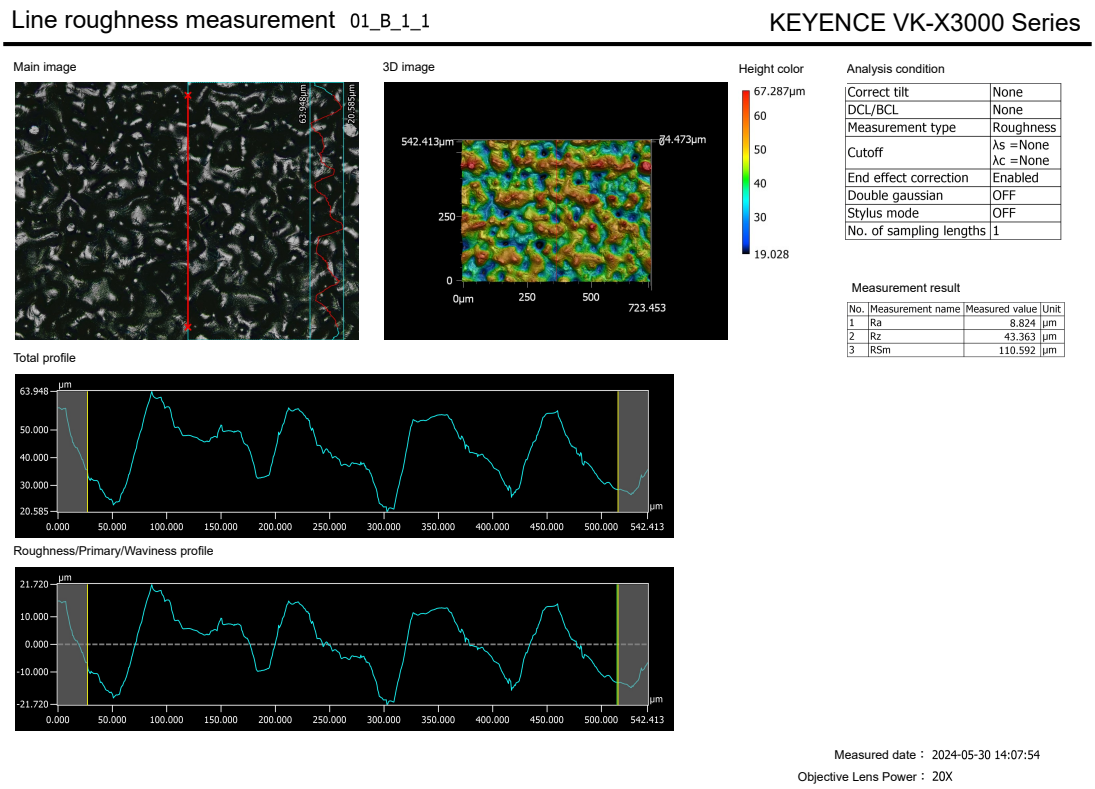

Figure B.2: Line roughness of surface 1 of 110GHz in Orientation 1

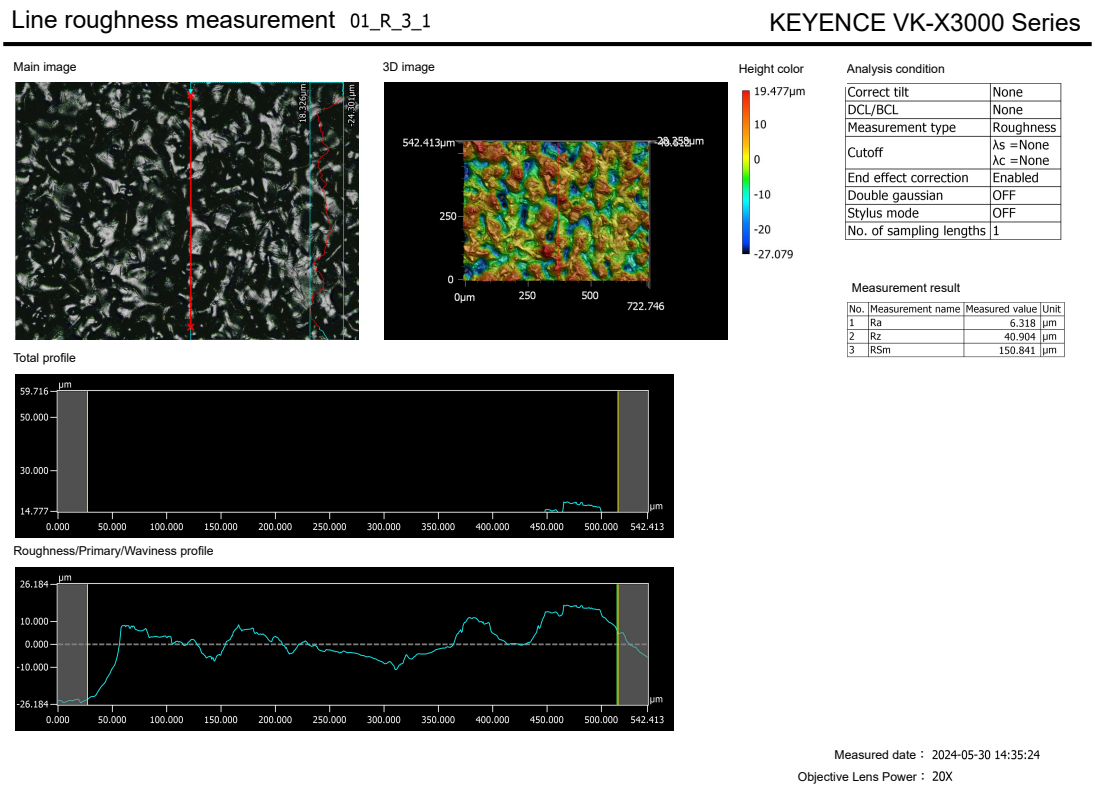

Figure B.3: Line roughness of surface 2 of 110GHz in Orientation 1

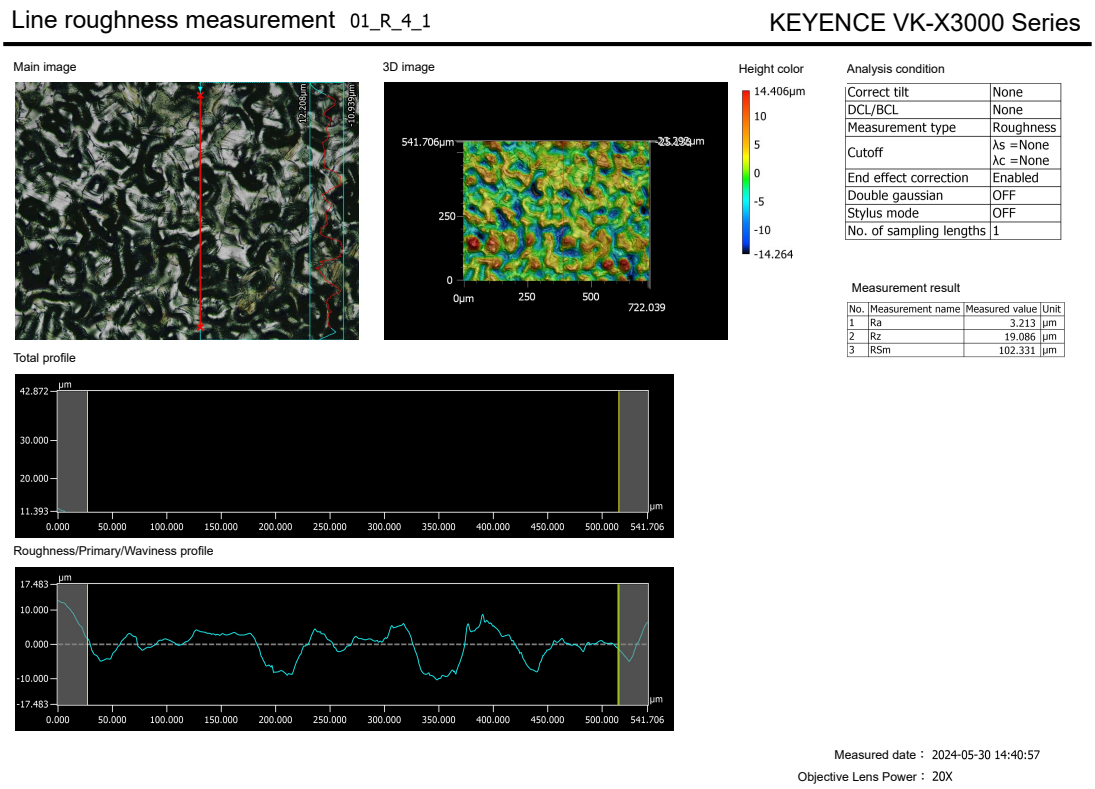

Figure B.4: Line roughness of surface 3 of 110GHz in Orientation 1

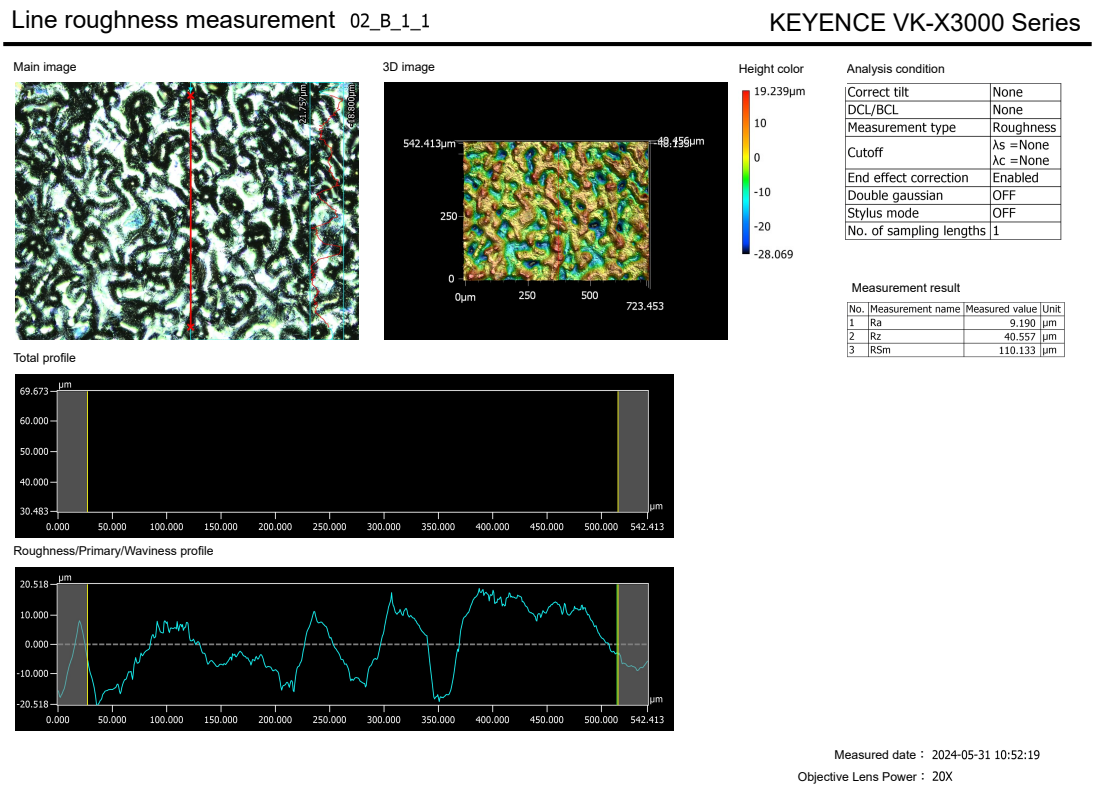

Figure B.5: Line roughness of surface 1 of 110GHz in Orientation 2

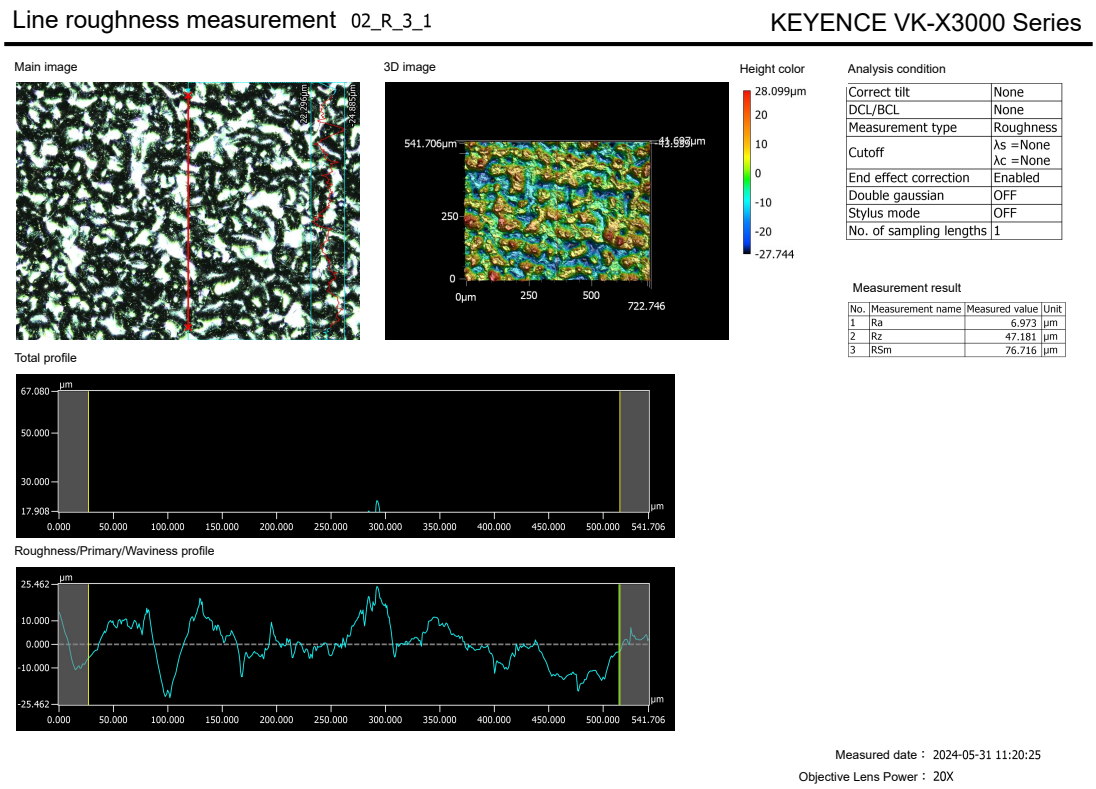

Figure B.6: Line roughness of surface 2 of 110GHz in Orientation 2

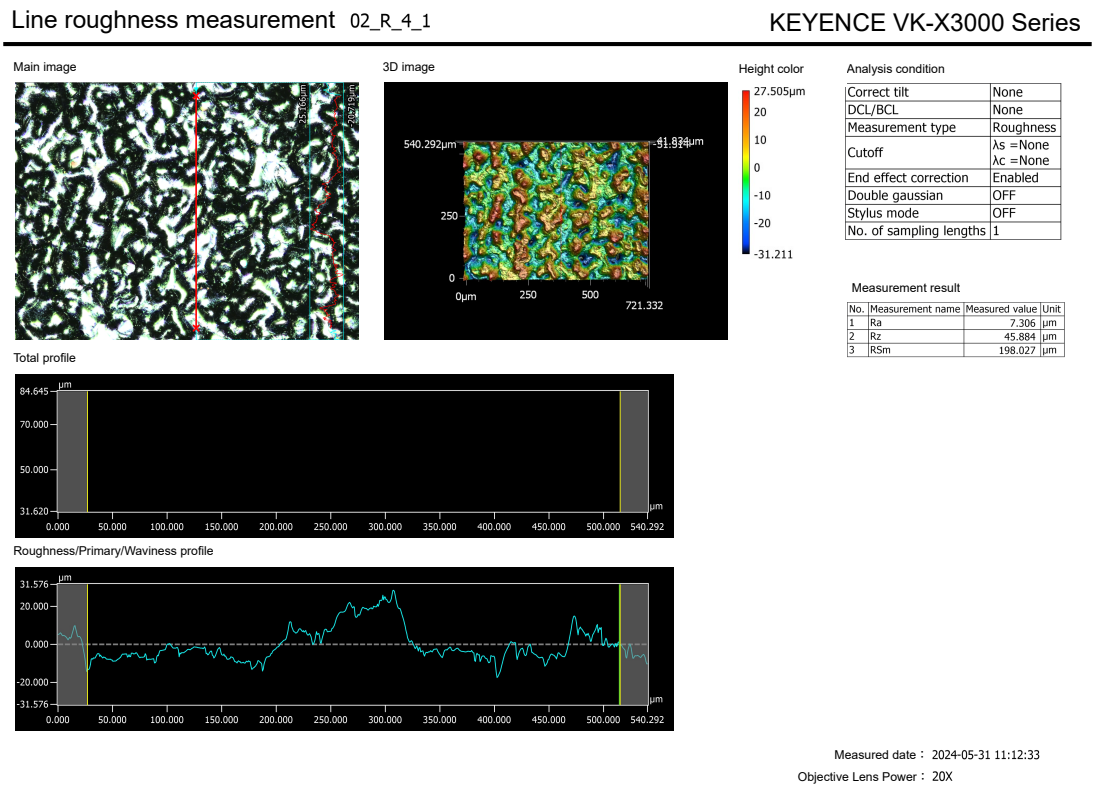

Figure B.7: Line roughness of surface 3 of 110GHz in Orientation 2

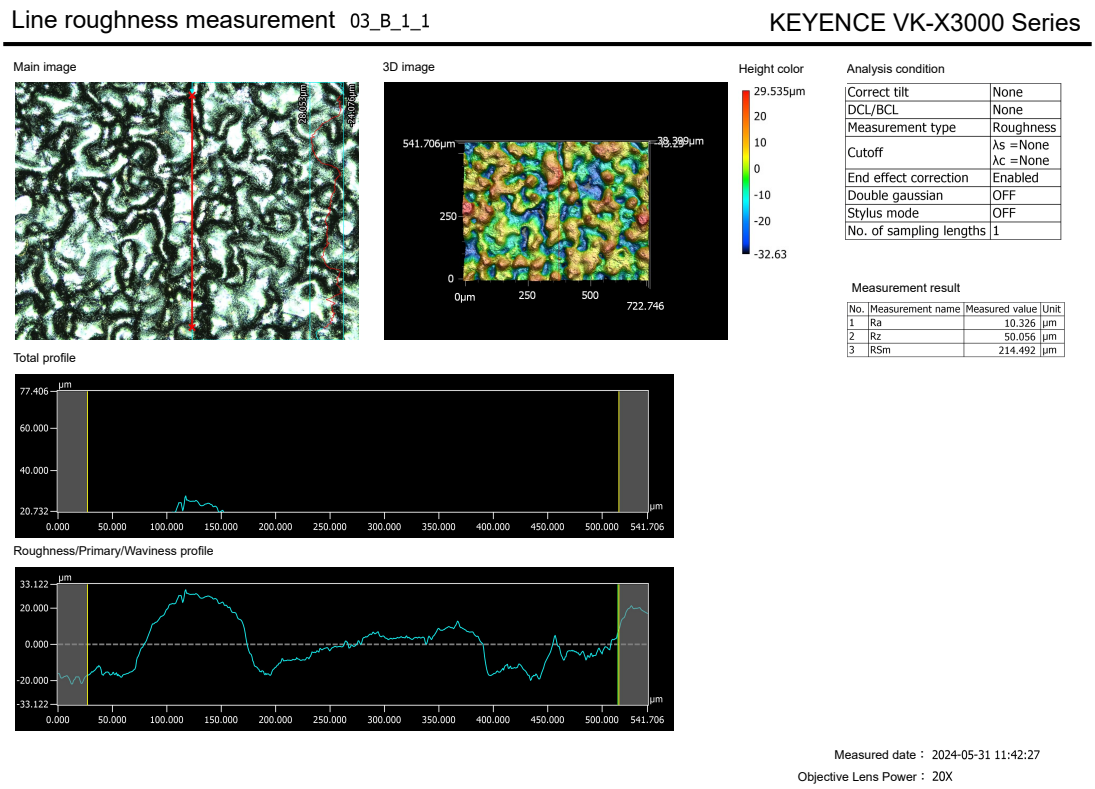

Figure B.8: Line roughness of surface 1 of 110GHz in Orientation 3

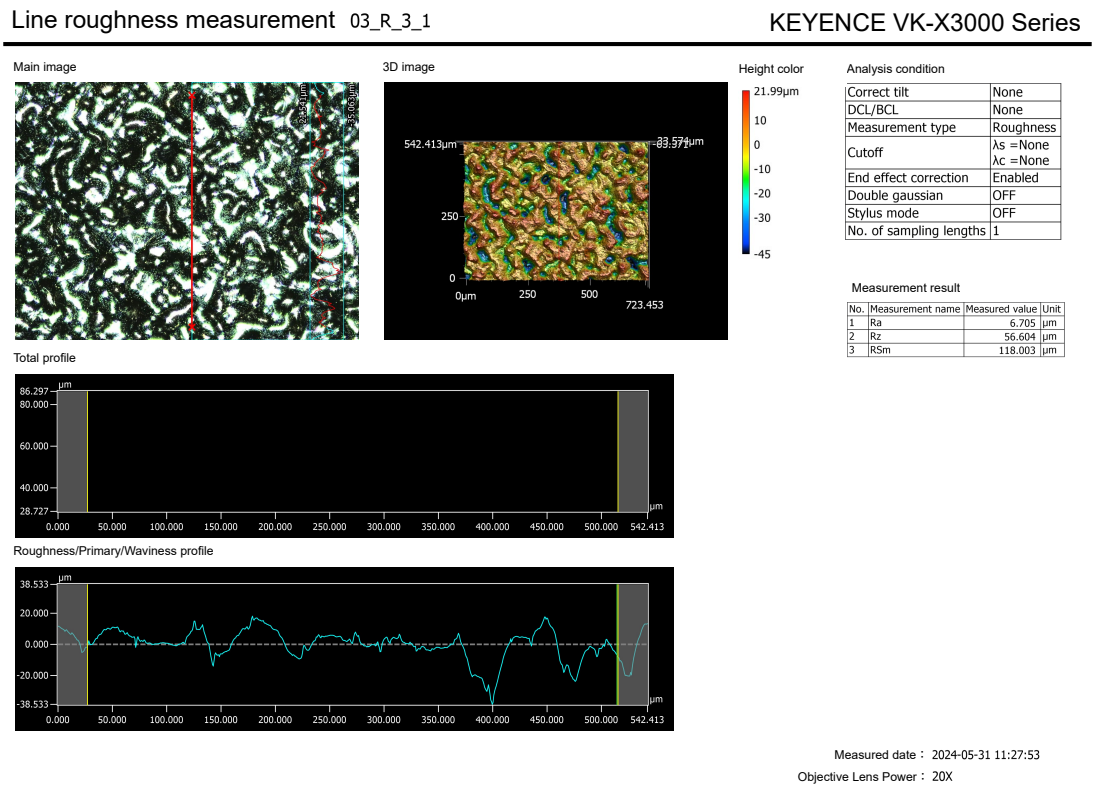

Figure B.9: Line roughness of surface 2 of 110GHz in Orientation 3

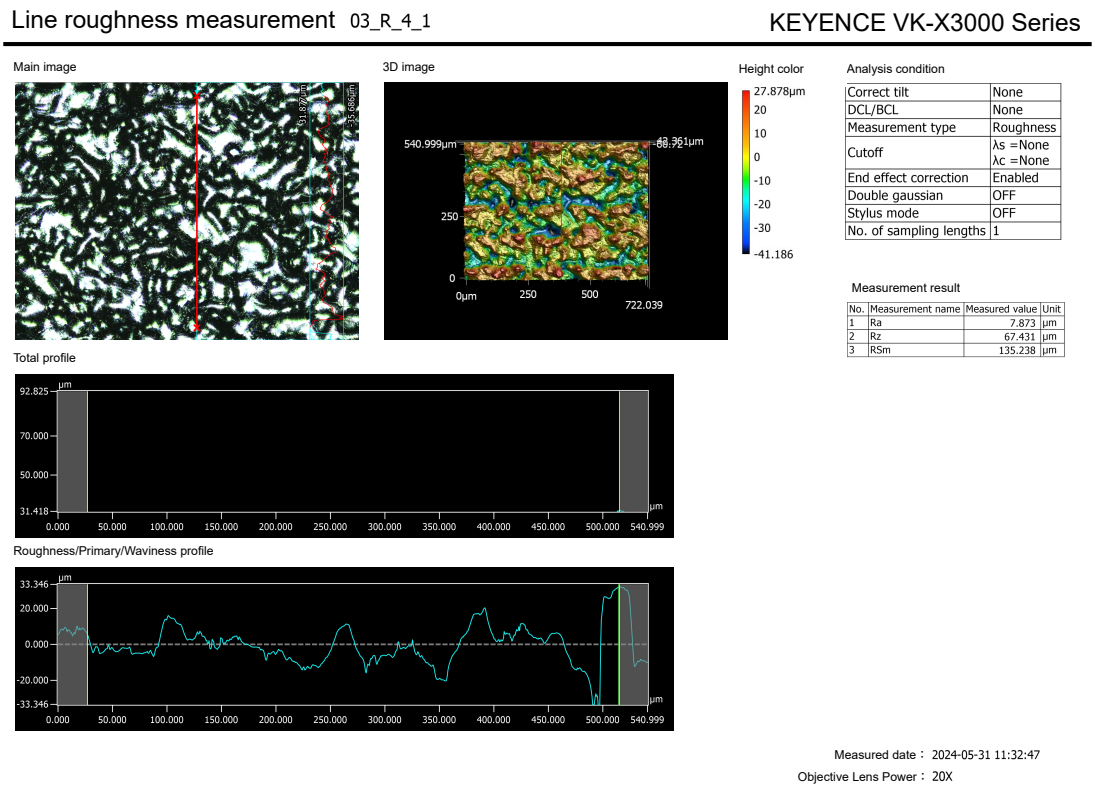

Figure B.10: Line roughness of surface 3 of 110GHz in Orientation 3

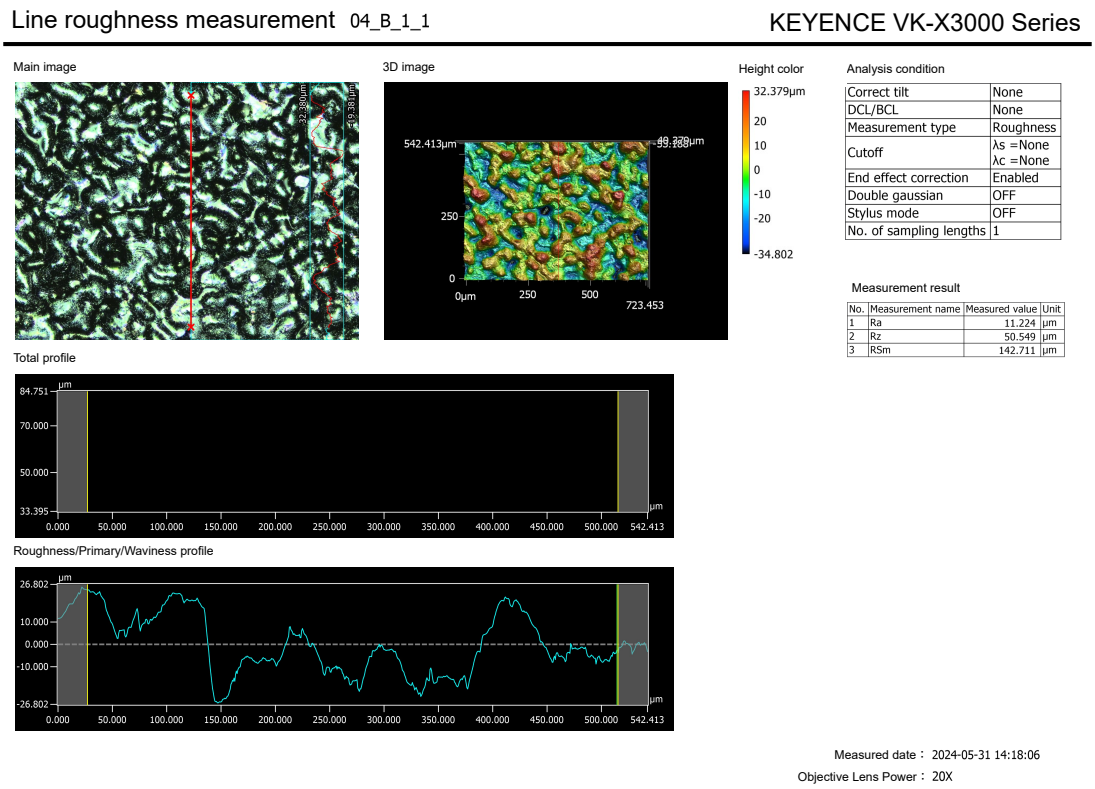

Figure B.11: Line roughness of surface 1 of 110GHz in Orientation 4

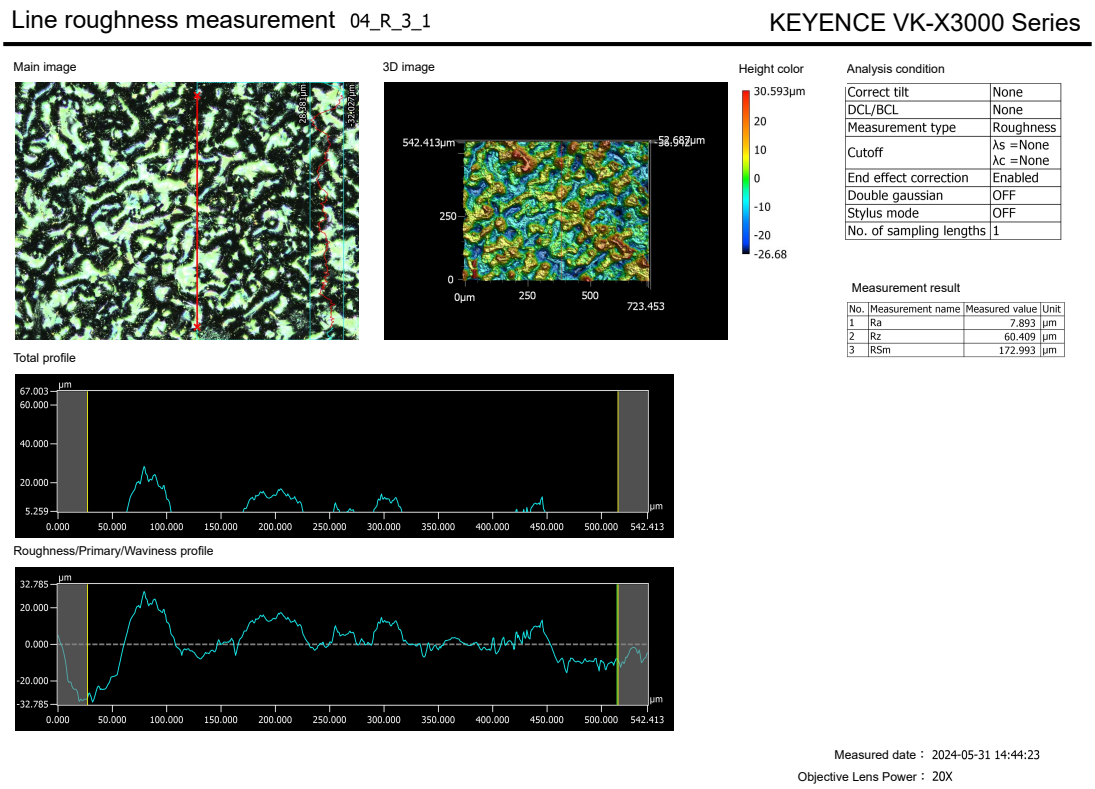

Figure B.12: Line roughness of surface 2 of 110GHz in Orientation 4

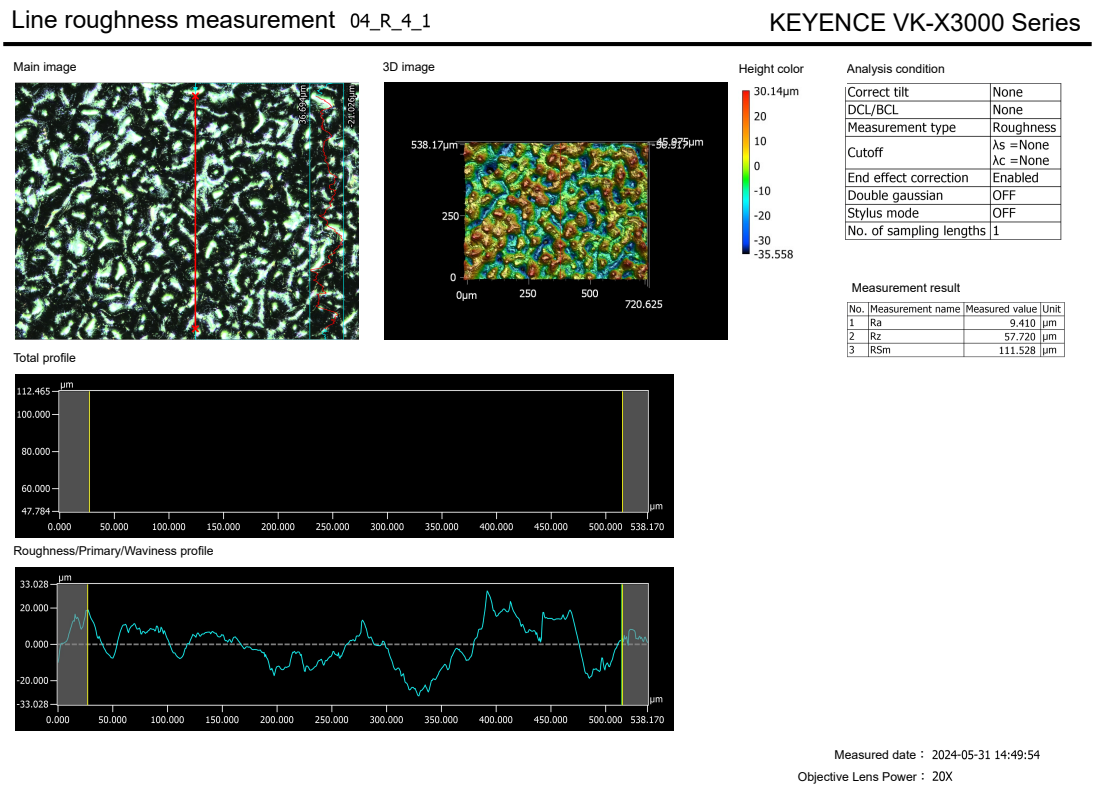

Figure B.13: Line roughness of surface 3 of 110GHz in Orientation 4

DEPARTMENT OF SOME SUBJECT OR TECHNOLOGY
CHALMERS UNIVERSITY OF TECHNOLOGY
Gothenburg, Sweden
www.chalmers.se

CHALMERS
UNIVERSITY OF TECHNOLOGY